Icarus 272 (2016) 258–276

Contents lists available at ScienceDirect

Icarus

journal homepage: www.elsevier.com/locate/icarus

Planetary period oscillations in Saturn's magnetosphere: Further comments on the relationship between post-equinox properties deduced from magnetic field and Saturn kilometric radiation measurements

S.W.H. Cowley*, G. Provan

Department of Physics and Astronomy, University of Leicester, Leicester LE1 7RH, UK

ARTICLE INFO

Article history:
Received 1 September 2015
Revised 20 November 2015
Accepted 26 February 2016
Available online 4 March 2016

Keywords:
Saturn
Magnetic field
Saturn, magnetosphere

ABSTRACT

We discuss the planetary period oscillations (PPOs) observed by the Cassini spacecraft in Saturn's magnetosphere, in particular the relationship between the properties of the PPOs in the post-equinox interval as observed in magnetic field data by Andrews et al. (2012) and Provan et al. (2013, 2014) and in Saturn kilometric radiation (SKR) emissions by Fischer et al. (2014, 2015), whose results are somewhat discrepant. We show that differences in the reported PPO periods, a fundamental property which should be essentially identical in the two data sets, can largely be accounted for by the phenomenon of dual modulation of the SKR emissions in polarization-separated data, in which the modulation associated with one hemisphere is also present in the other. Misidentification of the modulations results in a reported reversal in the SKR periods in the initial post-equinox interval, south for north and vice versa, relative to the magnetic oscillations whose hemispheric origin is more securely identified through the field component phase relations. Dual modulation also results in the apparent occurrence of phase-locked common periods in the northern and southern SKR data during later intervals during which two separate periods are clearly discerned in the magnetic data through beat modulations in both phase and amplitude. We further show that the argument of Fischer et al. (2015) concerning the phase relation between the magnetic field oscillations and the SKR modulations is erroneous, the phase difference between them revealing the local time (LT) of the upward field-aligned current of the PPO current system at times of SKR modulation maxima. Furthermore, this LT is found to vary significantly over the Cassini mission from dawn, to dusk, and to noon, depending on the LT of apoapsis where the spacecraft spends most time. These variations are consistent with the view that the SKR modulation is fundamentally a rotating system like the magnetic perturbations, though complicated by the strong LT asymmetry in the strength of the sources, and rule out a mainly clock-like (strobe) modulation as argued by Fischer et al. (2015), for which no physical mechanism is suggested. We also elucidate the nature of the magnetic periods, criticized by Fischer et al. (2015), which have previously been derived in ~100–200 day post-equinox intervals between abrupt changes in PPO properties, and further show that their argument that the magnetic phase data provide evidence for the occurrence of common phase-locked magnetic oscillations in some intervals is fallacious. The most important consequence of our results, however, is that they demonstrate the essential compatibility of the post-equinox magnetic field and SKR data, despite the contrary results published to date. They also show that due to the dual modulation effect in polarization-separated SKR data, analysis and interpretation may contain more subtleties than previously realized. Joint examination of the combined magnetic and SKR data clearly provides greater insight and enhanced confidence compared with analyses of these data sets individually.

1. Introduction

One of the central focuses of research on Saturn's magnetosphere during the Cassini era has been the phenomenon of the

* Corresponding author. Tel.: +44 1162231331; fax: +44 1162522770.
E-mail address: swhc1@ion.le.ac.uk, swhc1@le.ac.uk (S.W.H. Cowley).

http://dx.doi.org/10.1016/j.icarus.2016.02.051

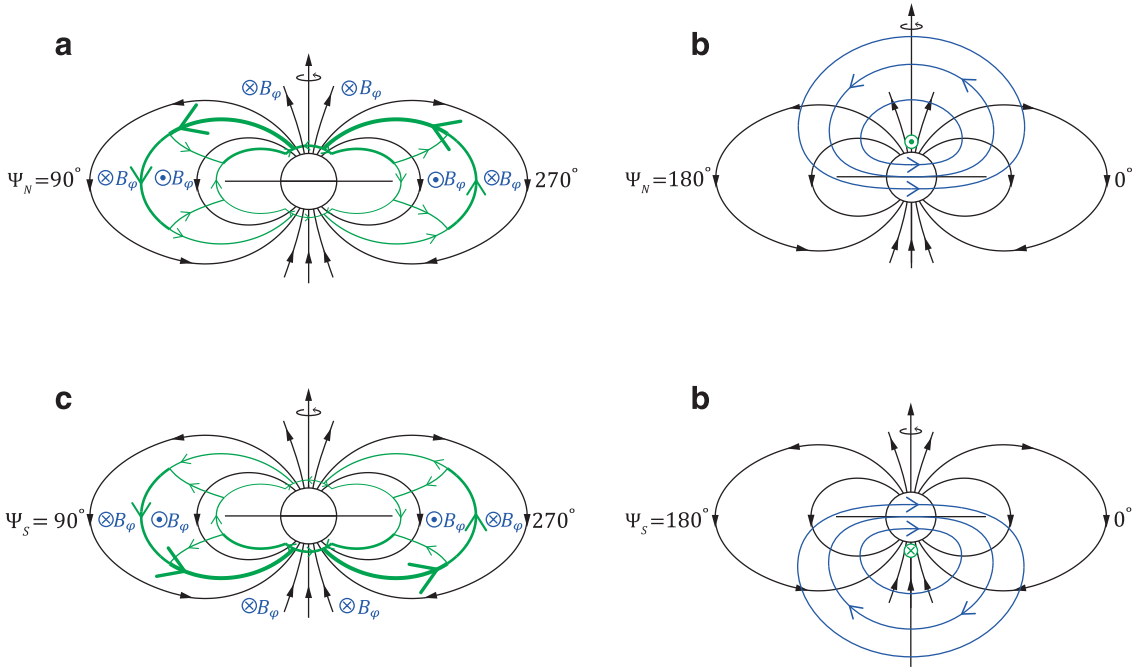

Fig. 1. Sketches showing the form of the electric currents and perturbation magnetic fields associated with the Saturn PPO phenomenon. Black arrowed lines show the background magnetospheric magnetic field, green arrowed lines and symbols the electric currents, and blue arrowed lines and symbols the associated perturbation magnetic field. Circled crosses and dots show vectors pointing into and out of the plane of the diagrams, respectively. Panels (a) and (b) show the northern PPO-related system, where panel (a) shows the $\Psi_N = 90^\circ - 270^\circ$ meridian plane and panel (b) the $\Psi_N = 0^\circ - 180^\circ$ meridian plane. Panels (c) and (d) similarly show the southern PPO-related system, where panel (b) shows the $\Psi_S = 90^\circ - 270^\circ$ meridian plane and panel (d) the $\Psi_S = 0^\circ - 180^\circ$ meridian plane. (Adapted from Hunt et al. (2015)) (For interpretation of the references to color in this figure legend, the reader is referred to the web version of this article.).

'planetary period oscillations' (PPOs) (e.g., Cowley et al., 2006; Southwood and Kivelson, 2007; Andrews et al., 2008, 2010a; Carbary et al., 2007; Provan et al., 2009; Burch et al., 2009; Kurth et al., 2008; Ye et al., 2010), in which modulations of the magnetic field, plasma populations, plasma waves, and radio emissions are observed throughout the system near the planetary rotation period of ~10.6 h despite the close axial symmetry of the planetary internal magnetic field (Burton et al., 2010). These studies have shown that modulations at two closely-spaced periods are usually present, one associated with the northern hemisphere and the other with the southern, which consideration of the observed magnetic signatures, together with modeling studies, suggests are due to two rotating current systems as sketched in Fig. 1 (Andrews et al., 2010b; Jia and Kivelson, 2012; Southwood and Cowley, 2014; Hunt et al., 2014). In these sketches (adapted from Hunt et al. (2015)) black lines indicate the axisymmetric background planetary magnetic field, green lines and symbols the electric currents, and blue lines and symbols the resulting perturbation magnetic field. Circled dots indicate vectors pointing out of the plane of the diagram, and circled crosses vectors pointing into the plane of the diagram. The sketches on the left (Fig. 1a and c) show the meridian plane of maximum field-aligned current for each system, while those on the right (Fig. 1b and d) show the resulting magnetic perturbations in an orthogonal meridian plane in which Fig. 1a and c are viewed from the left. In the northern system in Fig. 1a the principal field-aligned currents (thicker green lines) flow into the polar ionosphere on the right and out on the left, closing through the magnetospheric plasma and in oppositely-directed field-aligned currents at lower latitudes, producing a quasi-uniform perturbation field in the equatorial magnetosphere directed to the right in Fig. 1b, together with a quasi-dipolar closure field over the northern polar region. In the southern system in Fig. 1c the principal field-aligned currents flow into the ionosphere on the left and out on the right, similarly producing a quasi-uniform perturbation field in the equatorial magnetosphere directed to the right in Fig. 1d, together with a quasi-dipolar closure field over the southern polar region. The principal field-aligned currents are found to flow mainly on outer closed field lines, from near the open-closed field boundary inwards to ~9 R_S in the equatorial plane, essentially co-located with the main upward field-aligned currents associated with plasma subcorotation (Hunt et al., 2014, 2015). (R_S is Saturn's 1 bar equatorial radius, equal to 60,268 km.)

With increasing time these current systems rotate about the vertical axis with slightly different rotation periods, producing beats in the equatorial magnetosphere where the two quasi-uniform perturbation fields co-exist, but single periods over the two polar regions where the individual quasi-dipolar fields are uniquely present (Provan et al., 2011, 2012; Andrews et al., 2012; Hunt et al., 2015). Position with respect to these systems is defined by the northern (N) and southern (S) magnetic phases $\Psi_{N,S}$ around the spin axis as shown in Fig. 1, defined such that the equatorial quasi-uniform field points radially outward in each system where $\Psi_{N,S} = 0^\circ$ (on the right of Fig. 1b and d), and increases with time at a fixed point as the current system rotates in the sense of planetary rotation, by 360° for a full rotation. Brief study of these diagrams shows that for both systems the radial (r) field component then varies approximately as $\cos\Psi_{N,S}$, while the azimuthal (φ) component varies as $\sin\Psi_{N,S}$ in the equatorial region, in lagging quadrature with the r component, and as $-\sin\Psi_{N,S}$ in the polar regions, in leading quadrature with the r component. We note that these phase relations are characteristic of a quasi-uniform field in the equatorial region and of a transverse dipole in the polar region (Southwood and Kivelson, 2007; Andrews et al., 2008, 2010b, 2012; Provan et al., 2009). The co-latitudinal component, however, varies as $\cos\Psi_S$ in the southern system, in phase with the r component, but as $-\cos\Psi_N$ in the northern system, in antiphase with the r component (Andrews et al., 2008; Provan et al., 2011), a difference that allows separation of the two

perturbation fields in the equatorial data as discussed in Section 2. Although the basic phenomenology of the PPO-related systems has thus been delineated in recent studies, we note that the primary physical cause has yet to be firmly established, though appearing to involve rotating twin-vortex flows driven in the two polar thermospheres (e.g., Smith, 2010; Jia and Kivelson, 2012; Hunt et al., 2014).

The seasonally-varying properties of the PPOs have been monitored during the Cassini mission to date through measurements of the amplitude and phase of the magnetic oscillations associated with the rotating quasi-uniform perturbation fields observed on few-day periapsis passes through the quasi-dipolar 'core' region of the magnetosphere (dipole $L \leq 12$) on near-equatorial orbits, combined with corresponding measurements of the rotating quasi-dipolar perturbation fields on open field lines over the two polar regions on orbits that are sufficiently inclined. These data show that the periods were well-separated and slowly varying during Saturn southern summer early in the Cassini mission 2005–2008, at ~10.8 h for the dominant southern oscillations and ~10.6 h for the weaker northern oscillations, but converged towards a common period with near-equal amplitudes over a ~1.5 year interval centered near Saturn vernal equinox in mid-August 2009 (Andrews et al., 2008, 2010b, 2012). After near-coalescing at ~10.68 h in the second half of 2010, the periods were found to separate again, the southern ~10.69 h remaining longer than the northern ~10.64 h, while from early 2011 the amplitudes underwent a sequence of abrupt transitions at intervals of ~100–200 days from southern to northern dominance and vice-versa that continue to the present (Provan et al., 2013, 2014). Minor changes in period and phase generally occur at the same times.

The variations of the PPO properties have also been followed over the course of the Cassini mission through observations of the modulations of Saturn kilometric radiation (SKR) (Kurth et al., 2008; Gurnett et al., 2009, 2011; Lamy, 2011), a conically-beamed radio emission at kilometre wavelengths excited through cyclotron maser instability of accelerated auroral electrons (Lamy et al., 2010, 2011). It was through these modulations that the PPO phenomenon was first observed in Voyager radio data (Warwick et al., 1981; Gurnett et al., 1981), and through which the seasonally-varying periods were first discerned in remote observations by Ulysses (Galopeau and Lecacheux, 2000). Due to their conical beaming, northern emissions can be observed up to ~20° latitude in the south, and southern emissions up to ~20° latitude in the north, such that both can be observed within ±20° of the equator outside of a shadow zone extending to ~4 R_S in the equatorial plane (Lamy et al., 2008a, 2008b, 2009; Cecconi et al., 2009; Kimura et al., 2013). Within this region the northern and southern emissions can also in principle be distinguished through their state of circular polarization, right hand (RH) from the northern hemisphere and left hand (LH) from the southern, corresponding to the extraordinary mode (Lamy et al., 2010; Lamy, 2011). In addition, for near-equatorial observations outside the shadow zone, corresponding to a majority of the interval discussed in this paper, observable SKR sources are restricted by beaming to those within two narrow bands of LT, ~1 h wide, displaced ~4 h LT either side of the observing point (Lamy et al., 2008b, 2009; Cecconi et al., 2009). The variations in emitted SKR power are thought to be due to modulation of the auroral currents by the rotating PPO current system, with northern or southern maxima being associated with times when the upward current of the corresponding PPO system as shown in Fig. 1 is superposed on the sources observed, thus enhancing the auroral electron acceleration and consequent radio emission. If sources at all LTs were equally intense, this would result in SKR modulations whose phase depends directly on the LT of the observer, as for the magnetic field oscillations (Cowley et al., 2006; Andrews et al., 2010a). However, the source strength of SKR emissions is found to depend greatly on LT, being strongest in the post-dawn sector at ~8 h LT and weakest at antipodal LTs in the post-dusk sector (Lamy et al., 2009), the asymmetry possibly being associated with a LT-dependent quasi-static current system associated with the solar wind interaction on which the PPO currents are superposed (Southwood and Kivelson, 2009). This then leads to the expectation that SKR modulations should be nearly "clock-like", or "strobe", in a wide LT sector from post-midnight to noon via dawn dominated by the post-dawn sources, as deduced from initial Voyager observations (Desch and Kaiser, 1981; Kaiser et al., 1984). At other LTs, however, the SKR modulation phase should depend on the LT of the observer, though skewed towards the phase of the stronger post-dawn sources on either side of the antipodal LT (Andrews et al., 2011). This effect has not been taken into account in analyses of the SKR data, however, potentially leading to small ~10 s differences in period between magnetic field and SKR analyses when apoapsis, where the spacecraft spends most time, varies in LT within the non-strobe dusk sector (Andrews et al., 2011; Provan et al., 2014). As discussed in Section 3.3, such differences are comparable to the uncertainties in period determined from the magnetic field data.

During most of the pre-equinox interval, however, Cassini apoapsis was principally located on the dawn side of the planet where near-strobe SKR conditions are expected to prevail. Correspondingly, the pre-equinox periods deduced from the magnetic and SKR data have generally been found to be in excellent agreement, with a consistent relative phasing such that the equatorial quasi-uniform perturbation field of the southern system pointed tailward at southern SKR maxima, while that of the northern system pointed sunward at northern SKR maxima (Andrews et al., 2008, 2010a, 2010b, 2012; Provan et al., 2009, 2011). As seen from Fig. 1, this phasing implies that in this interval SKR maxima in each hemisphere occurred when the upward field-aligned current of the corresponding system is located in the dawn sector near where the most intense SKR sources lie, consistent with the above discussion. In the year following equinox, the southern SKR periods determined by Lamy (2011) and Gurnett et al. (2011) continue to agree well with the slowly declining southern magnetic period, though the relative phasing changes via a small apparent difference in the deduced periods (as above) such that the southern equatorial perturbation field then pointed sunward at southern SKR maxima (Andrews et al., 2011, 2012). This implies that southern SKR maxima are then observed when the southern upward field-aligned current lies in the dusk sector, consistent with a switch in spacecraft apoapsis from the dawn to the dusk sector that took place shortly before equinox, so that the otherwise dominant dawn sources could no longer be observed (Andrews et al., 2011). Rather less good agreement was found for the northern period post-equinox, however, with the period deduced from SKR observations increasing more rapidly than the magnetic to coalesce with the declining southern period in early 2010 (Gurnett et al., 2010, 2011; Lamy, 2011). The coalescence in period deduced from the SKR data thus occurred significantly earlier than that deduced from the magnetic field data, which occurred in the second half of 2010 (Andrews et al., 2012). The cause of this discrepancy has remained unclear.

Within the subsequent ~100–200 day post-equinox intervals between abrupt PPO changes that started in early 2011, however, piecewise analysis of the magnetic and SKR periods (to mid-2013) are again found to yield closely similar results, with a mean difference in period of ~14 s in instances where the periods could be determined in both data sets (Provan et al., 2014). The relative phasing of the magnetic and SKR modulations also continued to differ from that observed throughout the pre-equinox interval, the quasi-uniform field for the northern system at northern SKR maxima rotating from tailward to duskward, and the field for the

southern system at southern SKR maxima rotating from sunward to dawnward, as the spacecraft apoapsis rotated from dusk into the post-noon sector. With reference to Fig. 1 these field directions then indicate dominance of SKR sources near to noon, consistent with the picture presented by Andrews et al. (2011).

Most recently, however, Fischer et al. (2014, 2015) have proposed a rather different view of post-equinox PPO properties, based on an alternative approach to analyzing SKR data. Similar to the analyses of magnetic field data by Andrews et al. (2012) and Provan et al. (2013, 2014), the SKR results in the above-cited studies, e.g., by Lamy (2011) and Gurnett et al. (2011) employ statistical analysis of ~200 day segments of radio data, such that the results are somewhat smoothed over such time scales. By contrast, Fischer et al. (2014, 2015) follow the SKR modulations "by hand", supported by directional statistics analysis of the data, such that it is in principle possible to follow changes in phase and hence period on a much shorter ~10 day time scale. Unlike the magnetic field data and the previous analyses of SKR data, they suggest that the SKR PPO periods became reversed, southern period shorter than northern, directly after equinox until early 2010. After this the northern and southern SKR periods are found generally to become equal to each other and phase-locked between the two hemispheres to at least early 2013, including intervals when the magnetic data indicate the presence of clearly separated northern and southern periods. An exception occurred in a six month interval starting early in 2011 when two periods again became evident in the SKR data, which are closely similar to the on-going magnetic periods. This interval is associated with the first two abrupt PPO transitions noted by Provan et al. (2013) as mentioned above, which Fischer et al. (2014) attribute to the occurrence of the Great White Spot storm on-going at that time. Clearly, given the physical picture outlined above, large discrepancies considerably exceeding uncertainties of typically a few tens of seconds between the PPO periods deduced from the magnetic field and SKR data such as those described by Fischer et al. (2014, 2015) are unexpected and call for investigation. Cowley and Provan (2015) have already discussed the results presented by Fischer et al. (2014) for the ~2.5 year interval from the start of 2010 to mid-2012, and have suggested that the phase-locked common periods are likely due to an SKR phenomenon of uncertain physical origin previously reported in pre-equinox data by Lamy (2011), in which modulations associated with one polarization-separated 'hemisphere', can also appear in the modulations associated with the other. Here we will not reprise those comments in detail, but will focus particularly on the interval of "reversed" periods reported from analysis of the immediate post-equinox data. Fischer et al. (2015) further examine the phase relationships between the magnetic field and SKR modulations in the post-equinox interval, and argue that their results show that the SKR modulation is mainly clock-like (strobe) at all LTs, the prior results of Andrews et al. (2011, 2012) and Provan et al. (2014) described above notwithstanding. Here we will also discuss the evidence concerning this conclusion, and will show their arguments to be erroneous.

2. Overview of post-equinox magnetic and SKR modulation data

In Fig. 2 we present an overview of the PPO properties derived from magnetic field data, which we will then compare with corresponding values from SKR data. We concentrate, as in Fischer et al. (2015), on the four calendar years 2009–2012 spanning Saturn vernal equinox on 11 August 2009, marked by the vertical dotted line. Start-of-year markers are shown at the top of the plot, together with Cassini revolution (Rev) numbers defined from apoapsis to apoapsis and shown at the time of periapsis. Interval identifiers are also shown, marked by the vertical dashed lines in the figure, as will be discussed further below. Time along the bottom of the plot is shown in days, where $t = 0$ corresponds to 00 UT on 1 January 2004. The top three panels of Fig. 2 show spacecraft orbit data relevant to our discussion. Specifically, Fig. 2a shows the radial range encompassed by each Rev on a logarithmic scale indicated by vertical bars plotted at the time of periapsis, showing whether the orbit was near-circular or highly elliptical, while Fig. 2b shows the LT of spacecraft apoapsis plotted as black circles at the time of apoapsis, potentially indicating the LT of the dominant SKR sources which may be contributing. Fig. 2c then shows the latitude range encompassed by each Rev indicated by vertical bars plotted at the time of periapsis with the latitude at periapsis shown by the black circle, which indicates whether equatorial or polar magnetic PPO data are potentially available.

In Fig. 2d and e we plot the magnetic phase data, shown over two full cycles with each data point being plotted twice to aid visualization of data continuity. The solid circles show phase data obtained on each periapsis pass through the core region ($L \leq 12$) on near-equatorial orbits, corresponding to the region of quasi-uniform field perturbations inside of the main field-aligned currents where beat-modulated combined northern and southern oscillations are observed (see Fig. 1). The open circles show data obtained from selected segments on polar open field lines (indicated by the lack of warm or hot electrons) on inclined orbits near the beginning and end of the interval, where single oscillations are observed corresponding to the hemisphere concerned (see Provan et al. (2014) for details). The phase data are obtained by fitting the azimuthally rotating function

$$B_i(\varphi,\ t) = B_{0\,i} \cos\left(\Phi_g(t) - \varphi - \psi_i\right) \tag{1}$$

to the magnetic measurements, where $\Phi_g(t)$ is a guide phase corresponding to a fixed period τ_g close to that of the oscillations (i.e., $\Phi_g(t) = (360\ t/\tau_g)$ deg, where again $t = 0$ corresponds to 00 UT on 1 January 2004), and φ is azimuth measured from noon increasing in the sense of planetary rotation. The fit then determines the amplitude $B_{0\,i}$ and the relative phase ψ_i for each spherical polar field component $i = (r,\ \theta,\ \varphi)$ on each pass. The r component phases are shown by red symbols, with θ phases shown green, and φ blue. Typical uncertainties in these values are ~10° (Andrews et al., 2012; Provan et al., 2013). In Fig. 2d we plot the equatorial and northern polar phase data in 'N-format' relative to a guide phase with period 10.64 h, in which the r component phase is plotted as measured, while the phases of the other two components have been adjusted to lie on a common line for a pure northern oscillation (within measurement error), which then reveals the northern phase. That is, we plot the phase values $(\psi_i - \gamma_{i\,N})$ versus time, where by definition $\gamma_{r\,N} \equiv 0°$, while from the discussion of Fig. 1 in Section 1 we have $\gamma_{\theta\,N} = 180°$ for both equatorial and polar data, and $\gamma_{\varphi\,N} = +90°$ for the equatorial data and $\gamma_{\varphi\,N} = -90°$ for the polar data. Similarly, in Fig. 2e the equatorial and southern polar phase data are plotted in 'S-format' relative to a guide phase with period 10.70 h, in which the r component phase is again plotted as measured, while the phases of the other two components have been adjusted to lie on a common line for a pure southern oscillation, which then reveals the southern phase. That is, we plot the phase values $(\psi_i - \gamma_{i\,S})$ versus time, where again by definition $\gamma_{r\,S} \equiv 0°$, while according to the discussion in Section 1 we have $\gamma_{\theta\,S} = 0°$ for both equatorial and polar data, and $\gamma_{\varphi\,S} = +90°$ for the equatorial data and $\gamma_{\varphi\,S} = -90°$ for the polar data.

Andrews et al. (2012) determined running linear fits to the phase data in Fig. 2d and e taken 25 data points at a time, typically spanning ~200 days as indicated in Section 1, yielding the northern and southern phases in intervals D2 (polar data on pre-equinox inclined orbits) and E1 (near-equatorial data on post-equinox equatorial orbits), shown by the red and blue solid lines in Fig. 2d and e, respectively. These lines specifically join phase values

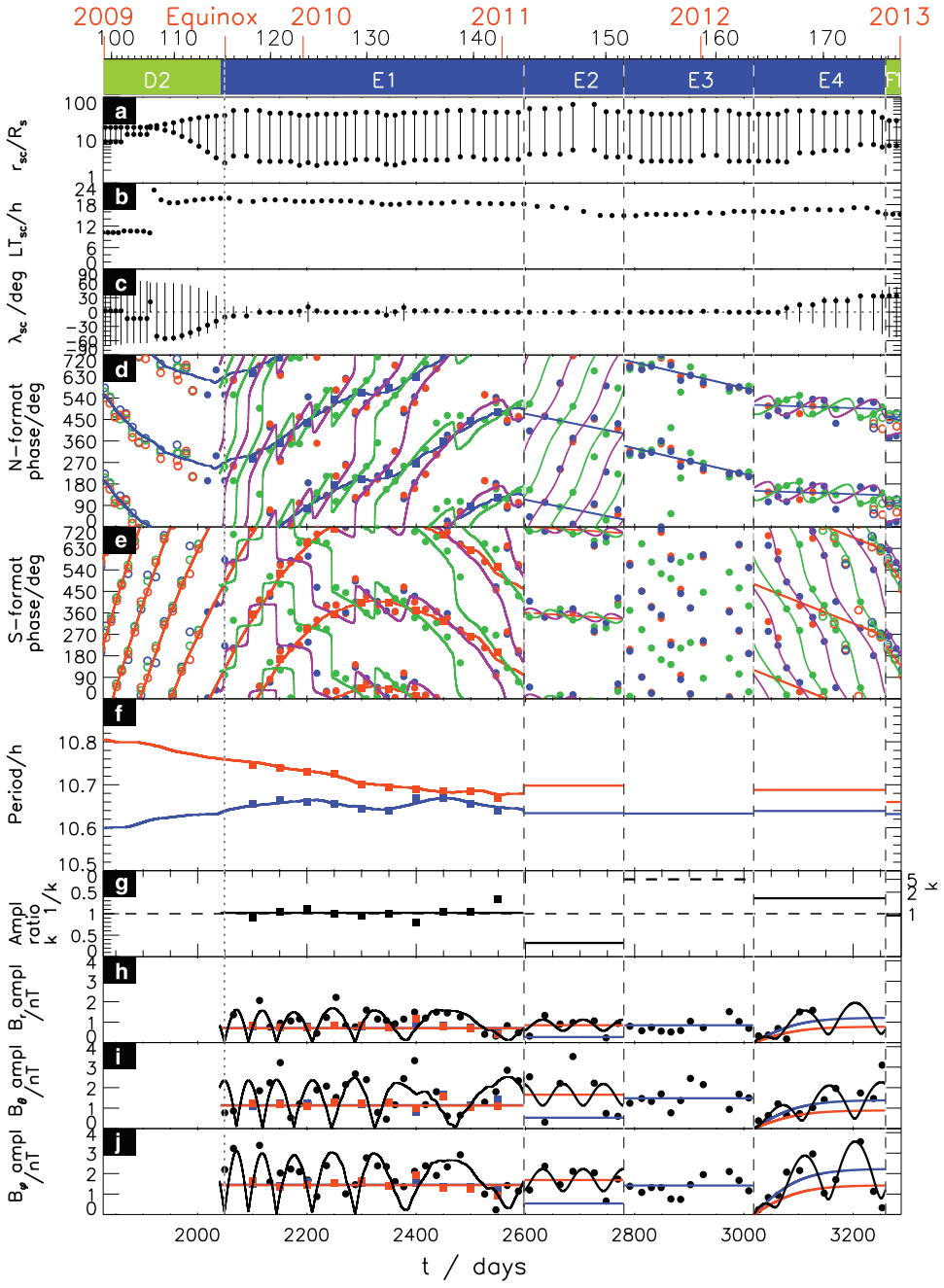

Fig. 2. Summary plot of Cassini orbit and magnetic PPO data over the four calendar years 2009–2012 inclusive. Year boundaries, Rev numbers plotted at periapsis, and interval identifiers are shown at the top of the plot, with the intervals also being marked by vertical dashed lines. The time of vernal equinox is also marked, shown by the vertical dotted line. Time t at the bottom of the plot is shown in days, with $t = 0$ corresponding to 00 UT on 1 January 2004. (a)–(c) Spacecraft orbital parameters, where (a) shows the radial range (R_S) on each Rev from periapsis to apoapsis plotted at the time of periapsis on a logarithmic scale, (b) the LT (h) of apoapsis, plotted at the times of apoapsis, and (c) the latitude range (deg) on each Rev plotted at the time of periapsis with the latitude of periapsis shown by the black circle. (d) The N-format phases of the magnetic oscillations ψ_N (deg) defined by Eq. (2) relative to a guide phase of 10.64 h period, where red, green, and blue data correspond to r, θ, and φ field components, respectively, shown over two cycles of phase with all data being plotted twice. The blue solid lines show the northern magnetic oscillation phases deduced by Andrews et al. (2012) in D2 and E1 and Provan et al. (2013) in E2-F1, the blue squares the values obtained independently in E1 from simultaneous 5-parameter fits with 50-day cadence to 150 day data segments by Provan et al. (2013), while the green and purple solid lines show the modeled beat-modulated phases of the N-format equatorial θ and (r, φ) component data, respectively, derived as described in the text. No beat modulation is shown in interval E3 since the southern phase cannot be discerned in the magnetic data. Panel (e) similarly shows the S-format phases of the magnetic oscillations ψ_S (deg) relative to a guide phase of 10.70 h period. The red solid lines show the southern magnetic oscillation phases deduced by Andrews et al. (2012) and Provan et al. (2013), the red squares the values obtained independently in E1 from simultaneous 5-parameter fits with 50-day cadence to overlapping 150 day data segments by Provan et al. (2013), while the green and purple solid lines show the modeled beat-modulated phases of the S-format equatorial θ and (r, φ) component magnetic phases. Panel (f) shows the corresponding oscillation periods, blue for the northern and red for the southern, where the solid lines and squares show values derived from magnetic field data by Andrews et al. (2012) and Provan et al. (2013). Panel (g) shows the north/south oscillation amplitude ratio k derived from magnetic field data in each near-equatorial interval (horizontal lines and squares), where the center dashed line indicates $k = 1$, with k plotted directly below the line ($0 \le k \le 1$), and ($1/k$) above ($1 \ge (1/k) \ge 0$). A k scale for the upper half panel is shown on the right of the plot. Panels (h)-(j) show amplitude data (black circles) for the r, θ, and φ field components, respectively, together with the individual northern (blue) and southern (red) amplitudes shown by the solid lines determined by Andrews et al. (2012) in E1 and Provan et al. (2013) in E2-E4. The squares in E1 show the 50-day cadence values determined by Provan et al. (2013). The black solid lines show the modeled beat-modulated combined amplitude, derived as described in the text. (For interpretation of the references to color in this figure legend, the reader is referred to the web version of this article.)

determined at the center time of each linear fit, typically spaced at intervals of ~10 days. The following intervals E2-E4 (mostly equatorial data) and F1 (mostly polar data) are then defined by the post-equinox abrupt changes in amplitude and period at intervals of ~100-200 days found by Provan et al. (2013) as also mentioned in Section 1, to which correspondingly only a single linear fit has been applied, similar in nature to each of the running ~200 day linear fits employed by Andrews et al. (2012). We note, however, that no southern phase is shown in interval E3 in Fig. 2e, since no phase clustering of the S-format data about some southern phase could be discerned in this case, generally indicating that the southern amplitude is less than ~20% of the northern, a limit set by the typical ~10° uncertainties in the fitted phases ψ_i noted above. The total northern and southern magnetic phases are then given by

$$\Phi_{N,S}(t) = \Phi_g(t) - \psi_{N,S}(t), \tag{2}$$

where $\psi_{N,S}(t)$ refers to the blue and red lines shown in Fig. 2d and e respectively. We note that this phase corresponds specifically to that of the r field component, plotted as measured in Fig. 2d and e, with the phases of the other components being simply obtained through use of the $\gamma_{i\,N,S}$ phase differences noted above. The period of the oscillations is then obtained from the gradient of the phase with respect to time

$$\tau_{N,S} = \left(\frac{360}{d\Phi_{N,S}/dt}\right), \tag{3}$$

where the phase is expressed in degrees. The northern and southern PPO periods thus derived from these magnetic phases are shown by the blue and red solid lines, respectively, in Fig. 2f.

As indicated above, the oscillations observed in the equatorial region (but not the polar) consist of the sum of northern and southern contributions

$$\begin{aligned} B_{0\,i}(t)\cos\left(\Phi_i(t)-\varphi\right) &= B_{0\,iN}\cos\left(\Psi_N(\varphi,\ t)-\gamma_{i\,N}\right) \\ &\quad + B_{0\,iS}\cos\left(\Psi_S(\varphi,\ t)-\gamma_{i\,S}\right) \\ &= B_{0\,iN}\cos\left(\Phi_N(t)-\varphi-\gamma_{i\,N}\right) \\ &\quad + B_{0\,iS}\cos\left(\Phi_S(t)-\varphi-\gamma_{i\,S}\right), \end{aligned} \tag{4}$$

where $\Psi_{N,S}(\varphi,\ t) = \Phi_{N,S}(t) - \varphi$ are the phase functions introduced in Fig. 1 in Section 1 which define azimuth relative to the rotating PPO current-field system, $\Phi_{N,S}(t)$ are the phases given by Eq. (2) which define the orientation of the current systems relative to noon (specifically the azimuth of the $\Psi_{N,S} = 0$ meridian where the r component is maximum, thus defining the direction of the equatorial quasi-uniform field), $B_{0\,iN,S}$ are the amplitudes of the two oscillations with north/south ratio $k = B_{0\,iN}/B_{0\,iS}$ assumed to be the same for each field component i (see Provan et al. (2011)), and $\gamma_{i\,N,S}$ are the constant angles given above that define the phase relationships between the three field components in each system. The phase $\Phi_i(t)$ of the observed combined equatorial oscillations in Eq. (4) is modulated about the individual phases $\Phi_{N,S}(t)$ at the beat period of the two oscillations, the modulations depending on both the beat phase $\Delta\Phi_B(t)$ given by

$$\Delta\Phi_B(t) = \Phi_N(t) - \Phi_S(t), \tag{5}$$

and the amplitude ratio k (Andrews et al., 2012; Provan et al., 2013). Given the phases $\Phi_{N,S}(t)$ of the two systems as indicated above, the value of k can then be found by fitting to the observed modulated phase values $\Phi_i(t)$. From a fit to the data for the whole of post-equinox interval E1 Andrews et al. (2012) found a value of $k = 1.02$ (i.e., near-equal amplitudes), while Provan et al. (2013, 2014) found k values of 0.32 (southern dominance) for E2, >5 (northern dominance with no detected southern modulation) for E3, 1.6 (weaker northern dominance) for E4, and 0.96 (near-equal amplitudes) for F1, respectively. These values are shown by the horizontal solid lines in Fig. 2g (dashed for the lower limit shown in E3), where the central dashed line marks equal amplitudes $k = 1$, and we show the value of k in the range $0 \le k \le 1$ in the lower half of the panel, and $1/k$ in the range $1 \ge 1/k \ge 0$ in the upper half of the panel (a k scale is also shown on the right of the plot), thus spanning the full range of k between zero and infinity.

Provan et al. (2013) also determined the phases $\Phi_{N,S}(t)$ and k values during E1 from simultaneous 5-parameter (two linear phases and k) fits to the observed phase data using 150-day data segments in overlapping intervals with centers separated by 50 days. The northern and southern phases so determined are shown by the blue and red squares in Fig. 2d and e, respectively, with periods similarly shown by the blue and red squares in Fig. 2f, while the k values are shown by the black squares in Fig. 2g. The phases and periods are seen to be very close to the essentially continuous values determined by Andrews et al. (2012), while the k values show modest variations about the single E1 $k \approx 1$ value determined by Andrews et al. (2012). The modeled modulated magnetic field phases in E1 shown in Fig. 2d and e by the green lines for the θ field component and by the purple lines for the r and φ components, are based on the Andrews et al. (2012) phases and the higher-resolution Provan et al. (2013) k values, where we have linearly interpolated the latter values between the points shown in Fig. 2g. In intervals E2-F1 only the single linear phases and the k values determined by Provan et al. (2013, 2014) have been used (except for E3 where no southern phase could be determined as indicated above). These model phases clearly give a good overall account of the beat-modulated phases observed in the equatorial magnetic data.

Having determined the northern and southern phases $\Phi_{N,S}(t)$ and the amplitude ratio k, we can also fit to the observed combined beat-modulated equatorial amplitudes $B_{0\,i}(t)$ in Eq. (4) to find the individual northern and southern oscillation amplitudes for each field component. In Fig. 2h–j the black solid circles show the observed amplitudes of the r, θ, and φ field components, respectively, while the blue and red lines show the northern and southern amplitudes, respectively, corresponding to the single values determined by Andrews et al. (2012) in E1 and by Provan et al. (2013) in E2-E4. We note that in E4 a hyperbolic tangent model has been employed to describe the recovery of the amplitude from its near-suppression at the beginning of that interval (Provan et al., 2013). The blue and red squares in E1 also show the 50-day cadence northern and southern amplitudes determined by Provan et al. (2013) (many of which near-overlap due to the $k \approx 1$ conditions prevailing). The solid black lines in Fig. 2h–j then show the modeled beat-modulated combined amplitudes, derived in E1 using the Andrews et al. (2012) phases and linear interpolations between the 50-day k and amplitude values determined by Provan et al. (2013), while in E2–E4 we use the single linear phases and k and amplitude values also determined by Provan et al. (2013). Although the amplitude data are somewhat noisy, beat modulations are clearly evident throughout (except for interval E3), that are generally well-described by the model values.

In Fig. 3 we show related PPO data derived from SKR measurements, and compare them with the magnetic field data in Fig. 2. Specifically, Fig. 3a and b show normalized smoothed SKR emission intensities taken from Fig. 12a and b of Fischer et al. (2015), respectively, where those in Fig. 3a show the RH circular polarized channel corresponding in principle to northern sources, while those in Fig. 3b show the LH circular polarized channel corresponding in principle to southern sources. Due to the SKR source visibility considerations mentioned in Section 1, the RH (northern) data are limited to intervals where the spacecraft latitude was northward of 20° south, while the LH (southern) data are limited to intervals where the spacecraft latitude was similarly southward of 20° north (Appendix B of Fischer et al. (2015)). Both intensities are thus simultaneously determined for near-equatorial data

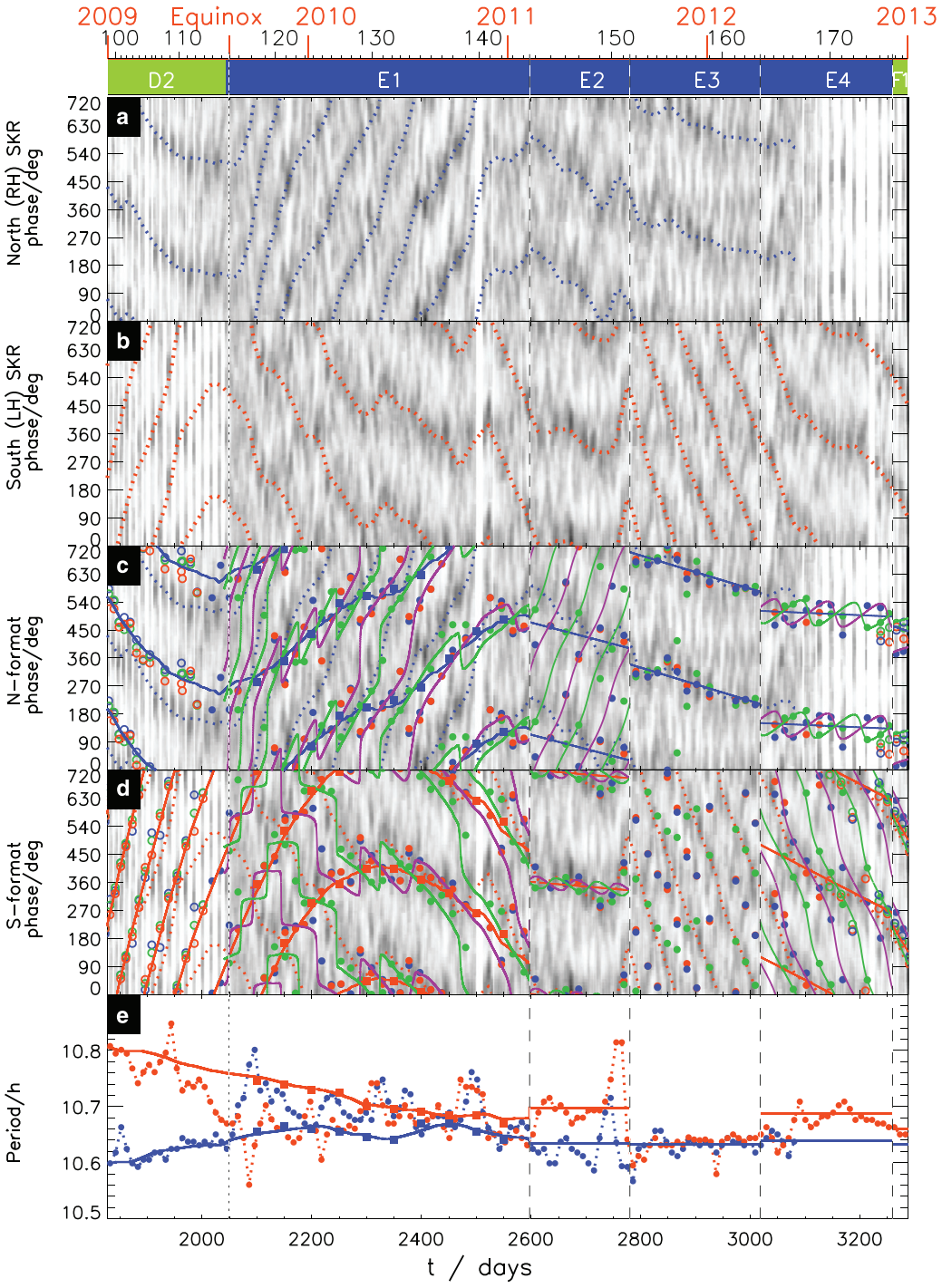

Fig. 3. Summary of Cassini SKR PPO data derived by Fischer et al. (2015) over the four calendar years 2009–2012 inclusive, together with a comparison with magnetic PPO data from Fig. 2, plotted in a similar format to Fig. 2. (a) Normalized smoothed gray-scaled northern (RH) SKR emission intensity data obtained from Fig. 12a of Fischer et al. (2015) plotted relative to a guide phase of 10.64 h period as in Fig. 2d, but displaced through −90° as discussed in the text. These data are shown here in negative format compared with Fig. 12a of Fischer et al. (2015) for ease of visibility of the over-plotted magnetic data shown in lower panels of the figure. The blue dotted line traces a line through northern SKR emission maxima (darkest pixels), showing the northern SKR phase ψ_N^* (Eq. (6)) derived by Fischer et al. (2015), shifted in phase by −90°. Two cycles of phase are shown to aid visualization of phase continuity, as in Fig. 2d. (b) Normalized smoothed gray-scaled southern (LH) SKR emission intensity data obtained from Fig. 12b of Fischer et al. (2015) plotted relative to a guide phase of 10.70 h period as in Fig. 2e, but now displaced through +90° as discussed in the text. The red dotted line shows the southern SKR phase ψ_S^* (Eq. (6)) which traces a line through southern emission maxima, also shifted by +90°. (c) We reproduce the northern (RH) SKR data shown in panel (a), but now superpose the N-format magnetic phase data and fitted model lines shown in Fig. 2d. Similarly (d) we reproduce the southern (LH) SKR data shown in panel (b), but now superpose the S-format magnetic phase data and fitted model lines shown in Fig. 2e. (e) A comparison of derived SKR and magnetic field PPO periods, blue for the northern and red for the southern, where the circles joined by dotted lines show SKR values associated with the SKR phases in panels (a)–(d) derived by Fischer et al. (2015) (Eqs. (6) and (7)), while the solid lines and squares show values derived from magnetic field data by Andrews et al. (2012) and Provan et al. (2013) (Eqs. (2) and (3)), as in Fig. 2f. (For interpretation of the references to color in this figure legend, the reader is referred to the web version of this article.)

when the spacecraft lay within 20° of the equator. These plots employ the same guide phase as for the magnetic data in Fig. 2d and e, respectively, with periods of 10.64 h for the RH (northern) data and 10.70 h for the LH (southern) data, and two cycles of phase are again shown on the vertical axis. However, for reasons to be discussed in Section 3.1, these SKR data have been shifted in phase relative to the magnetic data, by -90° for the RH data in Fig. 3a and by +90° for the LH data in Fig. 3b, as in Fig. 12a and b of Fischer et al. (2015). The intensities are shown gray-scale with darkest gray corresponding to the most intense emissions, this being the "negative" of the format shown by Fischer et al. (2015) in order to optimize visibility of the magnetic data shown over-plotted in Fig. 3c and d. Here the N- and S-format magnetic phase data and modeled phases shown in Fig. 2d and e are over-plotted on the northern (RH) and southern (LH) SKR intensities shown in Fig. 3a and b, respectively, for purposes of comparative discussion principally in Section 3.

The blue dotted lines in Fig. 3a and the red dotted lines in Fig. 3b then join sequences of elevated SKR intensities drawn "by hand" at 10 day intervals by Fischer et al. (2015), aided by directional statistics determinations using ~30 day segments of data, which serve to define the northern and southern SKR phases $\Phi^*_{N,S}(t)$, similar to the northern and southern magnetic phases $\Phi_{N,S}(t)$ given by Eq. (2). Here all quantities derived from SKR data will be indicated by a star. No SKR phases are shown for the northern data in Fig. 3a beyond $t = 3085$ days in mid-2012, however, due to the lack of continuous RH data on the southern-inclined orbits then occurring (Fig. 2c). It is readily shown (e.g., Appendix C of Fischer et al. (2015)) that the phases $\psi^*_{N,S}(t)$ defined by these lines are related to the SKR phases through a relation similar to Eq. (2) for the magnetic field data, i.e.

$$\Phi^*_{N,S}(t) = \Phi_g(t) - \psi^*_{N,S}(t), \tag{6}$$

where the SKR phases $\Phi^*_{N,S}(t)$ are such that northern and southern SKR maxima occur when $\Phi^*_{N,S} = 360N$ deg for successive integer N. However, due to the ±90° phase shifts introduced by Fischer et al. (2015) as mentioned above, the blue dotted line in Fig. 3a actually corresponds to $(\psi^*_N(t) - 90^\circ)$ while the red dotted line in Fig. 3b corresponds to $(\psi^*_S(t) + 90^\circ)$. From Eq. (6) the corresponding modulation periods are then given by

$$\tau^*_{N,S} = \left(\frac{360}{d\Phi^*_{N,S}/dt} \right), \tag{7}$$

shown by the blue (northern) and red (southern) circles joined by dotted lines in Fig. 3e.

Given the overview of SKR and magnetic PPO data in Fig. 3, we can now compare the derived properties, concentrating initially on the most obvious property of the PPO periods shown in Fig. 3e. On the left of the figure, in the immediate pre-equinox interval, it can be seen that a reasonable level of agreement exists between magnetic and SKR periods within a significant level of fluctuation in the latter data, as had been the case since the start of joint data in early 2005 (Andrews et al., 2012). Northern and southern periods are seen to converge from their well-separated pre-equinox values near ~10.6 and ~10.8 h, respectively. However, while the magnetic periods proceed to converge relatively smoothly to near-equal values around $t \approx 2400 - 2450$ days (early August to mid-September 2010), as did the periods derived from SKR data by Lamy (2011) and Gurnett et al. (2011) using ~200 day data segments, though with a somewhat earlier convergence in 2010 in those cases, the periods derived by the peak-tracking method adopted by Fischer et al. (2015) deviate from this behavior very markedly. Specifically, as the spacecraft orbit returned to the equatorial plane near to equinox (Fig. 2c), the two SKR periods appear to switch values around $t \approx 2050$ days (mid-August 2009), northern SKR to southern magnetic and vice versa, and to remain in that condition, within major fluctuations, until $t \approx 2300$ days (mid-April 2010). At that point the southern SKR period deduced by Fischer et al. (2015) resumes agreement with the southern magnetic period, while the northern SKR period continues near the southern magnetic period, such that the two SKR periods then have near-equal values. Fischer et al. (2014, 2015) show that the northern and southern SKR modulations also have near-equal phases (modulo 360°) during this interval, such that they appear to become "phase-locked" at a common period. Commonality with the southern magnetic period persists until $t \approx 2475$ days (early October 2010), when, after a short interval of significantly longer near-equal periods centered at $t \approx 2500$ days (early November 2010), the two phase-locked SKR periods become more closely equal to the northern magnetic period until the first abrupt change in PPO properties identified by Provan et al. (2013) occurred, near $t \approx 2600$ days (mid-February 2011). At that point, in interval E2, the two SKR periods separate again in good overall agreement with the magnetic field periods, though showing considerable short-term variations about the single values derived from the magnetic data. In interval E3 starting at $t \approx 2780$ days (mid-August 2011) phase-locked northern and southern periods are again deduced from the SKR data, having nearly the same value as the single northern magnetic field period, where we recall that no separate southern oscillation, e.g. near the on-going southern period in E2, could be discerned in the magnetic data. Subsequently, in interval E4 starting at $t \approx 3020$ days (early April 2012), phase-locked common periods which are closely comparable with the northern magnetic period continue to be deduced from the SKR data until the end of northern SKR data at $t \approx 3085$ days (mid-June 2011). After this time the southern SKR period increases sharply to become similar to the southern magnetic period, though declining gradually near the end of E4 at $t \approx 3260$ days (early December 2012) towards the smaller southern magnetic period derived in F2.

Given this initial comparison, we now outline four specific topics where the magnetic field results of Andrews et al. (2012) and Provan et al. (2013, 2014) are at issue with the SKR results presented by Fischer et al. (2014, 2015). Each of these topics will then be followed up in greater detail in the four sections in Section 3.

(a) Given the physical nature of the PPO phenomenon outlined in Section 1, in which the magnetic perturbations directly, and the radio emissions indirectly, result from the same rotating current system, the significant discrepancies in PPO periods deduced from the magnetic and SKR data in the interval following equinox are a major concern. The order of the expected uncertainty in period derived from clearly-banded N- or S-format magnetic phase data corresponds to a fraction of a rotation in the ~500 rotations that occur during the ~200 day intervals used to determine the period, thus amounting to uncertainties of a few tens of seconds. Uncertainties of similar order are quoted for SKR modulation periods determined over comparable intervals by Desch and Kaiser (1981) and Gurnett et al. (2005). Such uncertainties are, however, two orders of magnitude smaller than the ~10 min discrepancies in the periods determined by Fischer et al. (2015) in the immediate post-equinox data in interval E1 noted above. We mentioned in Section 1 that small differences in deduced period could arise due to the expected rotational nature of the SKR modulation phenomenon as observed in the dusk sector (Andrews et al., 2011), which is not taken into account in the SKR analysis. However, as indicated in Section 1, such differences are expected typically to be of order ~10 s, comparable with the uncertainties in the magnetic periods. Since we assert from physical principle that the periods associated with these phenomena cannot actually be different, apart from the effect of these small

deviations and measurement uncertainties, these results require examination and explanation. Later in interval E1, and with the exception of interval E2, phase-locked common periods are deduced from the SKR data to the end of joint data in mid-2012 as shown in Fig. 3e, despite separated dual periods clearly being present in the magnetic field data throughout E1 and in E4, as evidenced by the beat-modulated phases in Fig. 2d–f and the corresponding beat-modulated amplitudes in Fig. 2h–j. Phase-locked common periods are also deduced in E3, when the magnetic data show no evidence of southern oscillations. As mentioned in Section 1, Cowley and Provan (2015) have previously suggested that the phase-locked common SKR periods deduced by Fischer et al. (2014, 2015) are due to the phenomenon of uncertain physical origin first reported by Lamy (2011), in which SKR modulations associated with one hemisphere (i.e., one circular polarization state) also appear in the data associated with the other. In Section 3.2 we further examine this suggestion, and see how it may also provide some understanding of the "reversed" periods deduced from SKR data in the immediate post-equinox interval.

(b) Further on the topic of period determinations, in interval E2, when similar dual periods are deduced from both data sets, Fischer et al. (2015) criticize as "problematic" the single linear fits to the magnetic phase data and consequent single periods derived by Provan et al. (2013, 2014) shown in Fig. 2d-f, due to the variations in period seen in the higher cadence SKR data. They suggest that the uncertainties involved in the magnetic periods are much larger than those previously quoted, which are in accord with the outline discussion of uncertainties given above. In Section 3.3 we thus consider the physical meaning of the single periods deduced from the magnetic data, and their related uncertainties, and show that Fischer et al.'s (2015) criticisms are incorrect.

(c) Concerning the magnetic and SKR phases, Fischer et al. (2015) note the good agreement between the magnetic and ±90° shifted SKR phases that is evident in intervals E2-E4 in Fig. 3c and d where the periods are in overall accordance. They argue that this "agreement" is a direct consequence of the quadrature relation between the equatorial perturbation field and the field-aligned currents as shown in Fig. 1, and further suggest that this points to "a truly clock-like" (i.e., strobe) rather than a rotating SKR modulation (their Section 6.2). Elsewhere, however, they do show evidence for some rotating SKR signatures (their Section 5.1). In Section 3.1 we thus address the topic of the phase relations between the magnetic and SKR phases, and show that their discussion is significantly in error.

(d) Further concerning the phases, in interval E3 when no separate southern period could be discerned in the magnetic field data, Fischer et al. (2015) claim that the relationship between the southern SKR phase and the S-format magnetic phases seen in Fig. 3d provides direct evidence for the presence of a southern magnetic oscillation with the same period but in antiphase with the northern, compatible with the phase-locked common periods deduced from the SKR data. We consider their discussion in Section 3.4 and show that it is also in error. A related erroneous claim is also made in relation to the phase-locked periods deduced in interval E1.

3. Detailed discussion

In this section we now take up each of these four topics in more detail, beginning with discussion of the relative phase between the magnetic field oscillations and SKR modulations described by the functions in Eqs. (2) and (6), as outlined under point (c) in Section 2. This topic represents an appropriate starting point since it also has direct bearing on the discussion of the respective PPO periods outlined under point (a) in Section 2, taken up in Section 3.2.

3.1. Rotation effects in SKR phase data

In their Section 6.2, Fischer et al. (2015) argue that in the northern hemisphere the SKR maxima should lag the perturbation r component field maxima by 90°, on the basis that the upward field-aligned current carried by downward-going electrons in the northern PPO system lags the r component maxima by 90° (see Fig. 1a). Similarly, they argue that in the southern hemisphere the SKR maxima should lead the perturbation r component field maxima by 90°, on the basis that the upward field-aligned current in the southern PPO system leads the r component maxima by 90° (see Fig. 1c). We recall from Section 2 that the phase of the magnetic oscillations as defined by Eq. (2) is taken to relate specifically to that of the r component. Thus subtraction of 90° from the northern SKR phase, and addition of 90° to the southern SKR phase, as shown in Fig. 3a and b, respectively, should, they argue, bring the SKR phases into a "common line" with the magnetic phases in each case. This is indeed seen to be approximately the case in Fig. 3c and d for both the northern and southern phases in interval E2, as well as for the dominant northern phase in E3, and the weaker southern phase in E4 (as in Fig. 12 of Fischer et al. (2015)). As indicated under point (c) towards the end of Section 2, Fischer et al. (2015) further suggest that these results point to a "truly clock-like SKR source", i.e. a true SKR strobe, on the basis that the phase deviations associated with a rotating modulation, e.g., as discussed by Andrews et al. (2011), would generally cause a weakening in the level of agreement. In our view, however, the strobe scenario is clearly physically problematical since given the conically beamed nature of the SKR emissions and the consequent restrictions on the sources that can be viewed at a given point, this generally requires all sources to vary in concert independent of LT, for which no physical mechanism is suggested. Such a scenario would also lead to a fixed phase relation between the magnetic oscillations and the SKR modulations, contrary to the prior findings of Andrews et al. (2011, 2012) and Provan et al. (2014) outlined in Section 1.

The above argument given by Fischer et al. (2015) concerning the magnetic and SKR phase relationship is obviously erroneous, however, since the relationship between the field perturbations and the field-aligned current, governed only by Ampère's law, is independent of time, and has no direct connection with the temporal modulation of the SKR emission whose maxima occur at a specific magnetic phase, i.e., at a specific orientation of the current system relative to noon. Rather, as we now show, the differences between the (±90° shifted) SKR and magnetic phases for the northern and southern systems shown in Fig. 3c and d, respectively, directly give the azimuth with respect to noon of the upward field-aligned current in those systems at corresponding SKR maxima. Recalling that the magnetic phases $\Phi_{N,S}(t)$ by definition give the azimuth relative to noon at which the corresponding r component has a maximum at any time t, i.e., they give the direction of the quasi-uniform equatorial perturbation field, the corresponding upward field-aligned currents of these systems at that time (see Fig. 1a and c) are centered at azimuths $\varphi_{N,S}(t)$ given by

$$\varphi_N(t) = \Phi_N(t) - 90^\circ \quad \text{and} \quad \varphi_S(t) = \Phi_S(t) + 90^\circ. \tag{8a,b}$$

We also recall from Section 2 that the shifted northern and southern SKR phases shown in Fig. 3a–d correspond, respectively, to

$$\psi^*{}_N{}'(t) = \psi^*{}_N(t) - 90^\circ \quad \text{and} \quad \psi^*{}_S{}'(t) = \psi^*{}_S(t) + 90^\circ, \tag{9a,b}$$

on the basis of the argument given by Fischer et al. (2015) outlined above. Using Eqs. (2) and (6) the difference between the northern SKR and magnetic phases in Fig. 3c is thus given by

$$\Delta\psi'_N(t) = \psi^*{}_N{}'(t) - \psi_N(t) = \Phi_N(t) - (\Phi^*{}_N(t) + 90^\circ), \quad (10a)$$

where the equal guide phases have been eliminated, and noting that by definition $\Phi^*_N(t) = 0^\circ$ (modulo 360°) at northern SKR maxima, we thus find

$$\Delta\psi'_N(t) = \Phi_N(t) - 90^\circ = \varphi_N(t), \quad (10b)$$

i.e., the phase difference at northern SKR maxima is equal to the azimuth with respect to noon of the center of the northern upward field-aligned current at those times. Similarly, the phase difference between the southern SKR and magnetic phases in Fig. 3d is given by

$$\Delta\psi'_S(t) = \psi^*{}_S{}'(t) - \psi_S(t) = \Phi_S(t) - (\Phi^*{}_S(t) - 90^\circ), \quad (11a)$$

such that at southern SKR maxima where $\Phi^*_S(t) = 0^\circ$ (modulo 360°) we have

$$\Delta\psi'_S(t) = \Phi_S(t) + 90^\circ = \varphi_S(t), \quad (11b)$$

i.e., the phase difference at southern SKR maxima is equal to the azimuth with respect to noon of the center of the southern upward field-aligned current at those times. Thus the "agreement" between the SKR and magnetic phases noted in Fig. 3c and d (and in Fig. 12 of Fischer et al. (2015)) is essentially fortuitous, and, far from the discussion given by Fischer et al. (2015), means that the upward field-aligned currents of the two systems at corresponding SKR maxima in E2-E4 lie near to zero azimuth, i.e. are centered near to noon. This means that the quasi-uniform fields of the northern and southern systems at corresponding SKR maxima then point toward dusk and dawn, respectively (see Fig. 1a and c), entirely in line with the results reported previously by Provan et al. (2014) from an independent assessment of the phase relations between the post-equinox magnetic and SKR modulations (see their Section 3.3 and Fig. 7).

These relationships are not invariable throughout the Cassini data set, however, as would be required by the "clock-like" (strobe) SKR picture suggested by Fischer et al. (2015). In particular, during essentially the whole of the pre-equinox interval it was shown by Provan et al. (2011) and Andrews et al. (2011, 2012) that at northern and southern SKR maxima the upward field-aligned currents of the respective systems were centered near to dawn, such that the quasi-uniform perturbation field pointed towards noon for the northern system and towards midnight for the southern system at these times (Fig. 1a and c), as mentioned in Section 1. This effect is also seen directly in the pre-equinox data in Fig. 3c and d (interval D2), when the spacecraft apoapsis (as shown in Fig. 2b) was initially located in the pre-noon sector. The northern magnetic phases, not plotted by Fischer et al. (2015), then lie consistently ~90° above the well-observed northern SKR phases, and similarly but perhaps less consistently for the more intermittently observed southern SKR phases. This implies $\varphi_{N,S} \sim -90^\circ$ during interval D2, equivalent to ~270° modulo 360°, meaning that the upward currents at SKR maxima are then located at dawn. The phase "agreement" noted by Fischer et al. (2015) in E2-E4 is thus not invariable, showing directly that the SKR modulation is not in general "clock-like" as they suggest.

As shown by Andrews et al. (2011) and Provan et al. (2014), however, the changes observed in relative phase are consistent with the effect of a rotating SKR modulation associated with the rotating upward field-aligned currents of the PPO systems, combined with the strong LT asymmetry in the power of the auroral SKR sources. Taking account of the visibility of the conically beamed sources as outlined in Section 1, and assuming uniformly rotating modulations in emitted power which are proportional to the LT-dependent mean SKR power determined Lamy et al. (2009), Andrews et al. (2011) derived the effective modulation azimuth of the combined sources φ^* as a function of spacecraft azimuth φ_{SC} (their Fig. 2c), which Provan et al. (2014) showed could be approximated (modulo 360°) as

$$\varphi^* \approx 296^\circ + \left(\frac{180^\circ}{116^\circ}\right)\varphi_{SC}(\text{deg}) \quad \text{for} \quad 0^\circ \le \varphi_{SC}(\text{deg}) \le 232^\circ \quad (12a)$$

and

$$\varphi^* \approx 296^\circ \quad \text{for} \quad 232^\circ \le \varphi_{SC}(\text{deg}) \le 360^\circ. \quad (12b)$$

The effective SKR source azimuth φ^* given by Eq. (12) is shown by the solid line in Fig. 4, plotted versus φ_{SC}, with equivalent LT scales being shown at the top and right of the plot. For near-equatorial observation points at azimuths between 232° and 360°, corresponding to dawn-side LTs between ~3.5 h and ~12 noon, nearly clock-like (strobe) modulations are expected (Eq. (12b)), due to the dominance of post-dawn SKR sources peaking at $\varphi^* \approx 296^\circ$ (~7.7 h LT). This azimuth is shown by the horizontal dotted/solid line in Fig. 4 marked 'strobe'. In the opposite case of sources of equal strength at all LTs a uniform rotation would prevail with $\varphi^* = \varphi_{SC}$ for all φ_{SC}, shown by the inclined dashed line marked 'lighthouse'. Fig. 4 then shows that between 0° and 232°, i.e. from noon to ~3.5 h post-midnight via dusk, we expect a super-rotating lighthouse effect as given by Eq. (12a), in which the effective source azimuth is skewed away from the spacecraft azimuth towards the strobe azimuth on either side of its antipodal point at $\varphi^* \approx 116^\circ$ in the post-dusk sector.

If we further assume for highly elliptical spacecraft orbits (see Fig. 2a) that the azimuth of the spacecraft can be approximated as the azimuth of apoapsis where the spacecraft spends most time (Fig. 2b), and that SKR maxima occur when the upward field-aligned current of the corresponding PPO system is centered on the effective azimuth of the source at that spacecraft azimuth, then SKR maxima should correspond to times when

$$\varphi_{N,S} \approx \varphi^*(\varphi_{SC}), \quad (13)$$

where the right hand side is evaluated from Eq. (12) specifically using the spacecraft azimuth at apoapsis. Since from Eqs. (10) and (11) the difference between the SKR and magnetic phases in Fig. 3c and 3d are given by the azimuth of the upward field-aligned current at SKR maxima, $\Delta\psi'_{N,S} = \varphi_{N,S}$, the expected values of the SKR phases in these figures $\psi^*_{N,S}{}'(t)$ are given in terms of the magnetic phases $\psi_{N,S}(t)$ by

$$\psi^*{}_{N,S}{}'(t) \approx \psi_{N,S}(t) + \varphi^*(\varphi_{SC}), \quad (14)$$

where again the right hand side is evaluated from Eq. (12) using the spacecraft azimuth at apoapsis.

In Fig. 5a and b we show the magnetic (solid lines) and SKR (dotted lines) phases over-plotted on the gray-scale normalized smoothed SKR intensities for the northern and southern PPO systems, respectively, as in Fig. 3c and d, but now we also show the expected SKR phases from Eq. (14) based on the magnetic phases and the expected effective SKR source azimuth $\varphi^*(\varphi_{SC})$, plotted as solid circles at the time of each spacecraft apoapsis and joined by dotted lines. The small differences between the derived magnetic and SKR periods arising from the SKR rotational effects mentioned in Section 1 correspond to the differences in the slopes of the magnetic phases and the expected SKR phases given by Eq. (14) (see Eq. (3)). It can be seen from Fig. 2a–c that at the beginning of the interval the spacecraft was in an inclined elliptical orbit with apoapsis in the pre-noon sector, such that the strobe phase given by Eq. (12b) then applies, i.e., $\varphi^* \approx 296^\circ$ (equivalent to -64° modulo 360°) associated with dominant post-dawn SKR sources. The expected displacement of the SKR phases to smaller values

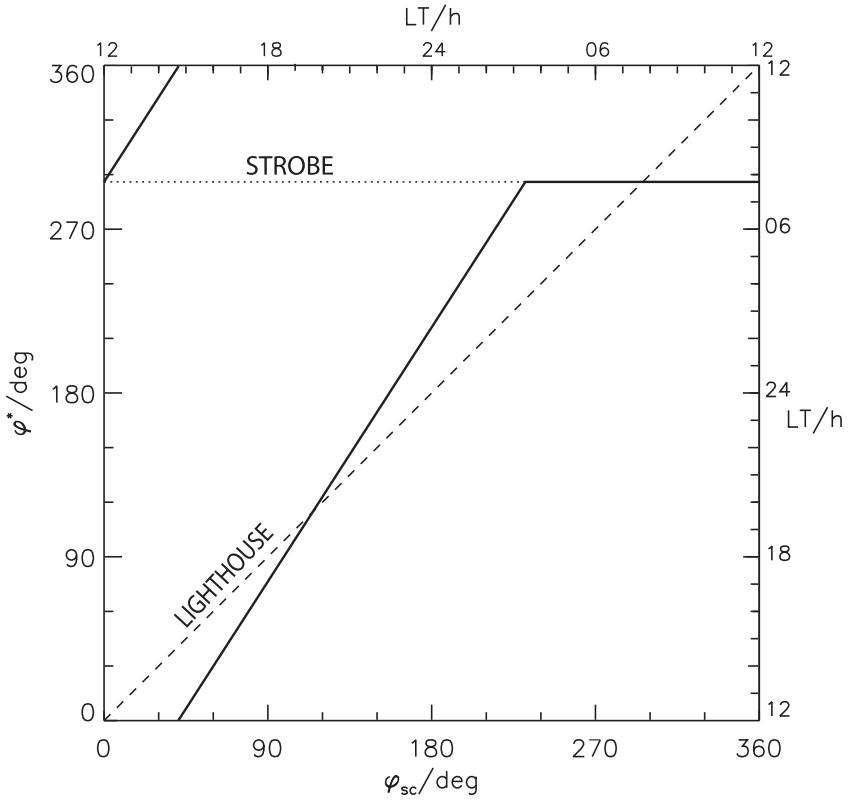

Fig. 4. Plot showing the effective azimuth measured from noon of the auroral SKR sources φ^* (deg) versus the azimuth of the observing spacecraft φ_{SC} (deg), obtained in simplified form from Eq. (12) (following Provan et al. (2014)), based on Fig. 2c of Andrews et al. (2011). Equivalent values of LT are given at the top and on the right scales of the plot. The horizontal dotted line marks the 'strobe' azimuth corresponding to the strongest post-dawn SKR sources, which dominate the observed emissions between ~3.5 and 12 h LT in the dawn sector. The 45° inclined dashed line marked 'lighthouse' indicates the case that would pertain for sources of equal strength at all LTs, in which case $\varphi^* = \varphi_{SC}$.

than the magnetic is then clear for the well-observed northern SKR emissions in Fig. 5a, as noted above, though generally suggesting a dominant source at somewhat earlier LTs, nearer to dawn, than given by the simple model. A similar effect is also seen in Fig. 5b for the less well-observed southern emissions after $t \approx 1900$ *days*. Subsequently, however, apoapsis underwent a sudden pre-equinox switch into the dusk sector via an interval of near-circular orbits, during which the dawn SKR sources appear to remain dominant as shown. Post-equinox, however, the orbit became near-equatorial and highly elliptic with apoapsis initially in the post-dusk sector (Fig. 2a–c), and since Eq. (14) was derived primarily to apply to data under such conditions, post-equinox we show results obtained directly from the formula. On this basis we expect a switch in the displacement of the SKR maxima to larger phases relative to the magnetic phases by ~90° throughout interval E1, as shown by the solid circles with dotted lines. The relationships between the SKR and magnetic phases in E1, during which large discrepancies exist in deduced PPO periods as noted in Section 2 (Fig. 3e), will form the topic of Section 3.2 below.

During following intervals E2-E4 when the periods are again in good general agreement, however, we note that the spacecraft apoapsis rotated from dusk to pre-noon across E2, and remained in that sector, with small variations, for the remainder of the interval (Fig. 2b). The expected SKR phase displacement from the magnetic phases shown by the solid circles with dotted lines in Fig. 5a and b then reduces to small positive values across E2, and remains at similar small positive values across E3 and E4. We note from Eq. (12a) and Fig. 4 that the phase displacement is expected to be zero, i.e. $\varphi^* \approx 0^\circ$ with the effective SKR source azimuth at noon, when $\varphi_{SC} \approx 40^\circ$ (~15 LT) in the post-noon sector. These phases are then seen to be in good accordance with the SKR data, showing that the "agreement" deduced by Fischer et al. (2015) on the basis of their erroneous argument is actually due to near-noon effective SKR sources when the spacecraft apoapsis is in the post-noon sector. We note that similar post-noon apoapsis conditions also occurred for a short interval earlier in the Cassini mission, during the second half of 2007 (interval C of Andrews et al. (2012)), when the phase relationship between SKR and magnetic field phases was again consistent with dominant near-noon SKR sources, with the quasi-uniform field of the northern system pointing towards dusk and that of the southern system towards dawn at corresponding SKR maxima (see Fig. 2 of Andrews et al. (2012) or Fig. 2 of Provan et al. (2014)). The results shown here, together with those discussed previously by Andrews et al. (2011, 2012) and Provan et al. (2014), are thus consistent with predictions given approximately by Eqs. (12)–(14) for a rotating modulation of SKR sources as previously deduced by these authors, and show conclusively that the SKR modulations are not predominantly clock-like (strobe) as concluded by Fischer et al. (2015).

3.2. Magnetic and SKR phases and periods in post-equinox interval E1

While the PPO phases and periods deduced from magnetic field and SKR emission data in pre-equinox interval D2 and post-equinox intervals E2–E4 are thus in good overall agreement, having allowed for SKR rotational effects, the correspondences are more varied in initial post-equinox interval E1, as outlined in Section 2. Approximately reversed dual periods, north for south and vice versa, were deduced by Fischer et al. (2015) from the SKR data in the first part of the interval, followed by phase-locked common northern and southern SKR periods that first approximate the

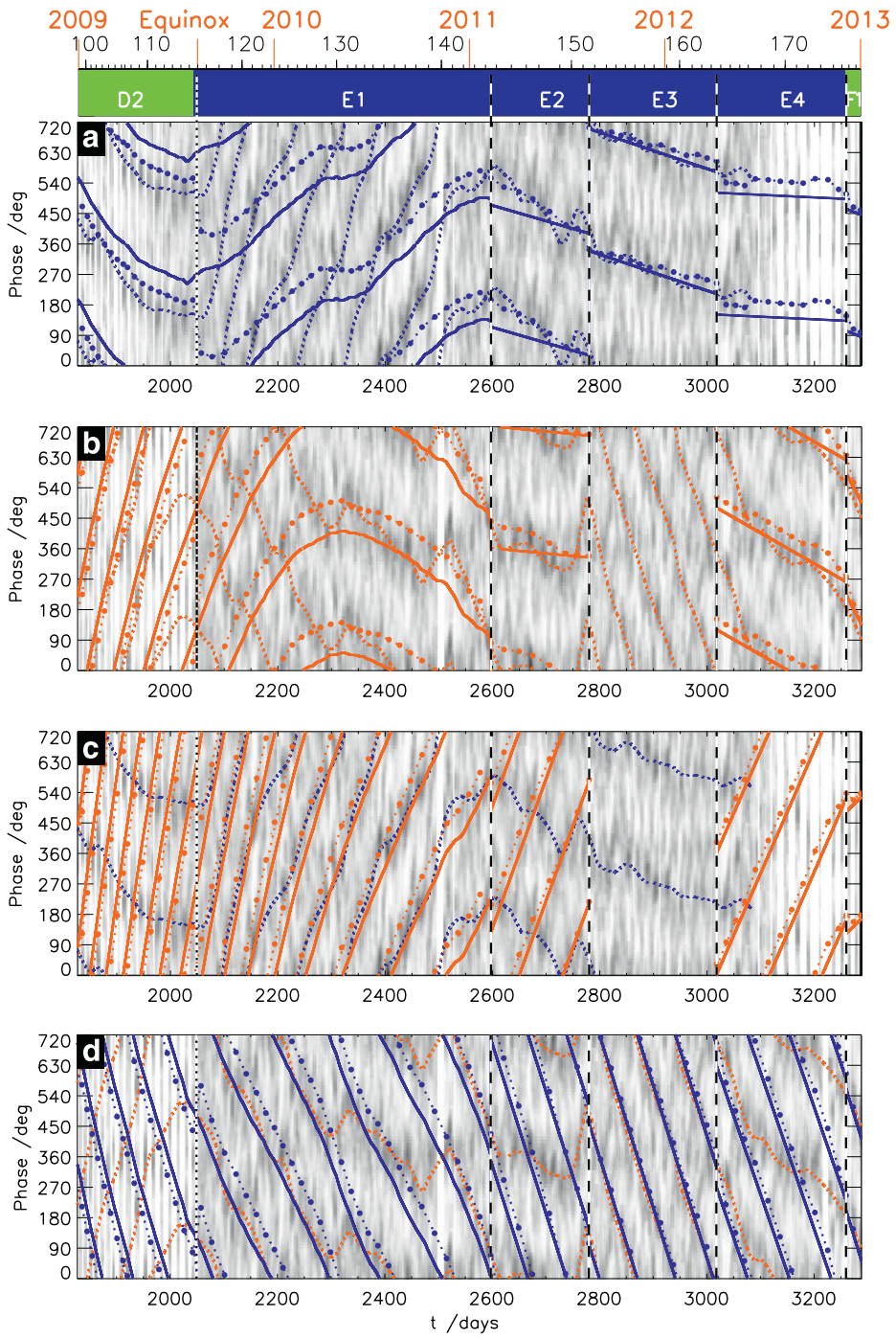

Fig. 5. Plots of magnetic field and SKR phase data for the four year interval 2009–2012 inclusive, shown in a format similar to Fig. 3c and d. (a) Phase data are over-plotted on normalized smoothed RH polarized (northern) SKR intensity data plotted relative to a guide phase with period 10.64 h and shifted by −90°, where the blue dotted lines show the northern SKR phase deduced by Fischer et al. (2015) (Fig. 3a and c), the blue solid lines the northern magnetic field phase deduced by Andrews et al. (2012) (D2 and E1) and Provan et al. (2013) (E2-F1) (Figs. 2d and 3c), while the blue circles (plotted at apoapsis) joined by dotted lines show the expected phase of the northern SKR modulation maxima based on the northern magnetic phase and the location of the spacecraft according to the approximated theory of Andrews et al. (2011) given by Eqs. (12)–(14). (b) Phase data over-plotted on normalized smoothed LH polarized (southern) SKR intensity data plotted relative to a guide phase with period 10.70 h and shifted by +90°, where the red dotted lines show the southern SKR phase deduced by Fischer et al. (2015) (Fig. 3b and d), the red solid lines the southern magnetic field phase deduced by Andrews et al. (2012) (D2 and E1) and Provan et al. (2013) (E2-F1) (Figs. 2e and 3d), while the red circles (plotted at apoapsis) joined by dotted lines show the expected phase of the southern SKR modulation maxima based on the southern magnetic phase and the location of the spacecraft. Panel (c) is similar to panel (a) and again shows the RH polarized (northern) SKR intensity and deduced phase (blue dotted line) as before, but now shows the southern magnetic phase data in panel (b) (red symbols and lines) transformed in guide phase from a period of 10.70 to 10.64 h and offset in phase by 180° such that the red circles joined by dotted red lines show the expected location of southern SKR emission maxima in the northern (RH) data. Panel (d) is then similar to panel (b) and shows the LH polarized (southern) SKR intensity and phase (red dotted line) as before, but now shows the northern magnetic data in panel (a) (blue lines and symbols) transformed in guide phase from a period of 10.64 to 10.70 h and offset in phase by 180° such that the blue circles joined by dotted blue lines show the expected location of northern SKR emission maxima in the southern (LH) data. (For interpretation of the references to color in this figure legend, the reader is referred to the web version of this article.)

southern magnetic period in the middle of the interval and then the northern magnetic period towards its end (Fig. 3e). On the other hand, separated dual periods are clearly present in the magnetic data throughout as evidenced by the beat-modulation of both phases and amplitudes seen in Fig. 2d and e, and 2h–j, except possibly for the brief interval of near-coalescence in period centered near $t \approx 2425$ days (late August 2010). Here we now examine the joint magnetic and SKR data in E1 in more detail, bearing in mind the general principle that the periods associated with these two phenomena cannot actually be different, outside of the small differences associated with the rotational effects discussed in detail in Section 3.1, so that some accommodation must exist.

Examining first the southern (LH polarized) SKR data in Fig. 5b, it can be seen that the SKR phases in E1 drawn by Fischer et al. (2015) initially follow distinct bands of enhanced SKR intensity that move to smaller phases with increasing time over the interval $t \approx 2050 - 2300$ *days*, showing that the corresponding period is smaller than the guide period of 10.70 h. Eq. (7) shows that the period is ~10.65 h, and thus in the vicinity of the northern magnetic period at that time as shown in Fig. 3e. However, a rising band of enhanced SKR emission is also present in this interval, with notable peaks in intensity at intervals of ~100 days near ~2125, ~2200, and ~2300 days, which approximately follow the location of southern SKR maxima expected on the basis of the southern magnetic phases as shown by the red circles with dotted lines. These are the southern (LH) SKR enhancements that are approximately followed in previous determinations of the southern SKR modulation phase during this interval by Lamy (2011) and Gurnett et al. (2011) (see Fig. 3b of Fischer et al. (2015) and related discussion), with consequent derived periods that are close to the southern magnetic period rather than close to the northern period as for the Fischer et al. (2015) southern SKR phase. It can be seen that these maxima occur near to times when the falling banded enhancements followed by the Fischer et al. (2015) southern SKR phase cross the expected southern emission maxima based on the magnetic data, and that the Fischer et al. (2015) phases flatten and rise in their vicinity, corresponding to increases in deduced period close to and somewhat above the 10.70 h guide period, as shown by the quasi-periodic increases of southern SKR period in Fig. 3e.

In order to examine the origin of the Fischer et al. (2015) southern SKR phases in this interval, in Fig. 5c and d we show the SKR emission data and Fischer et al. (2015) SKR phases as before in Fig. 5a and b, respectively, but we now superpose the southern magnetic phases in the northern (RH polarization) plot in Fig. 5c, and the northern magnetic phases in the southern (LH polarization) plot in Fig. 5d, both transformed relative to the corresponding guide phases. In order to account for the $\pm 90°$ shifts introduced into the SKR data and phases by Fischer et al. (2015), as described in Sects. 2 and 3.1 above, we have also shifted the magnetic phases in each plot by 180°, such that the solid circles with dotted lines show where SKR emission maxima are expected to occur in these plots if southern emission maxima occur in the northern (RH) data (Fig. 5c) and northern emission maxima occur in the southern (LH) data (Fig. 5d), based on the magnetic phases. It is immediately seen from Fig. 5d that the falling bands identified by Fischer et al. (2015) in the southern SKR data during this interval, $t \approx 2050 - 2300$ *days*, correspond closely to expectations of where northern modulation maxima would occur in the southern data based on the northern magnetic phase, but with a somewhat smaller positive offset from the latter, suggesting northern SKR sources at somewhat earlier LTs nearer noon than indicated by the simple model (Eqs. (12)–(14)). Overall, it can therefore be seen that the southern (LH) SKR data in this interval contain both southern and northern modulations, of which the studies by Lamy (2011) and Gurnett et al. (2011) emphasize the former, while the study by Fischer et al. (2015) picks out the latter. The results in Fig. 5 show that these dual SKR modulations are in good agreement with expectations based on the northern and southern magnetic data in accordance with our statement of physical principle in Section 2, the hemispheric provenance of which is more securely identified from the field component polarization characteristics and physical picture in Fig. 1. The quasi-periodic southern SKR period variations deduced by Fischer et al. (2015) in this interval together with the overall emission enhancements noted above occur approximately at times when the two modulations are in phase, roughly at the ~70 day beat period of the magnetic oscillations then prevailing.

Following this initial interval in E1, the southern SKR phase in Fig. 5b is then in approximate agreement with the southern magnetic phase over $t \approx 2300 - 2475$ *days*, with a similar period in Fig. 3e as noted above and in Section 2, though the positive phase offset from the magnetic phase declines from the expected value shown by the red circles with dotted lines early in the interval towards zero at its end, again possibly suggestive of a motion of the dominant SKR sources from the dusk sector towards earlier LTs near noon. In Fig. 5d there is no clear sign of continuing northern modulation in the southern SKR data during this central interval of E1. After this, however, the northern modulation reasserts itself in the southern SKR data across the data gap centered near $t \approx 2500$ *days*, which the Fischer et al. (2015) SKR southern phase then follows closely to the end of interval E1 at $t \approx 2600$ *days*, as shown by the blue circles with dotted lines in Fig. 5d. We note from Fig. 5b, however, that the expected southern maxima are approximately co-located with the northern during this interval ($t \approx 2500 - 2600$ *days*), though with a distinctly longer period than the northern, as shown in Fig. 3e. We further note that the brief interval of distinctly longer southern SKR periods ~10.75 h in Fig. 3e deduced by Fischer et al. (2015) centered near the SKR data gap at $t \approx 2500$ *days*, and the associated interval of sharply rising southern SKR phases in Fig. 5b and d, appears to originate as the SKR phase switches from following the southern magnetic phase in the central interval of E1 to following the northern magnetic phase again at its end. Overall, these results demonstrate variable dual modulation of the southern (LH) SKR emissions at both northern and southern magnetic periods during E1, leading to the apparent, but physically impossible, disparate magnetic and SKR results discussed by Fischer et al. (2015).

We now similarly examine the northern SKR modulations and phases in E1 in light of these results, as shown in Fig. 5a and c. It can immediately be seen from Fig. 5c that the rising bands of enhanced emission that define the Fischer et al. (2015) northern SKR phases in these figures, thus at longer period than the guide period of 10.64 h, correspond closely to expectations based on the southern magnetic period throughout the interval $t \approx 2050 - 2500$ *days*. The only exception occurs in a short interval centered near $t \approx 2200$ *days*, when the banding in the SKR data becomes temporarily less distinct such that the Fischer et al. (2015) northern phase segues between adjacent cycles of southern magnetic phase, leading to a brief interval of reduced northern SKR period closer to the guide period, as seen in Fig. 3e. Somewhat surprisingly, only modest evidence is seen for superposed modulations at the northern magnetic period in these data, though peaks in emission appear to occur near to the expected phase shown by the blue circles, positively offset from the northern magnetic phase, near to times when the northern and southern modulations are expected to be in phase, at ~2150, ~2200, ~2300, and ~2400 days. Following this interval, however, the northern (RH) SKR emission maxima and deduced phase then switches across the SKR data gap near $t \approx 2500$ *days* to correspond to expectations based on the northern magnetic phase to the end of interval E1, as in the southern hemisphere at that time, though with a slightly smaller positive phase offset from the magnetic phase. We note that the switch in deduced SKR phase across the data gap near $t \approx 2500$ *days* from

following the southern magnetic phase to following the northern, again results in a temporary but significant spurious increase in the derived northern SKR periods to ~10.75 h at this time, as seen in Fig. 3e.

Overall, these results are consistent with the prior suggestions of Cowley and Provan (2015) that in the central interval of E1 ($t \approx 2300 - 2500$ *days* corresponding to mid-April to early November 2010) the SKR modulations observed in both hemispheres (polarization states) agree with expectations based on the southern magnetic phase, though with some indications of northern modulation in the northern (RH) data, while in the later interval of E1 ($t \approx 2500 - 2600$ *days* corresponding to early November 2010 to mid-February 2011) both agree with expectations based on the northern magnetic phase. We note that centrally within the former of these intervals, corresponding to interval E1-7 of Provan et al. (2013) spanning $t = 2325 - 2475$ *days*, the north/south magnetic amplitude ratio k was found to be 0.80, corresponding to modest southern dominance, while during the latter interval, corresponding to interval E1-10 spanning $t = 2475 - 2625$ *days*, the ratio was found to be 1.33, corresponding to modest northern dominance (see the data indicated by the black squares in Fig. 2g). During the earlier interval $t = 2050 - 2300$ *days*, however, corresponding to intervals E1-1 to E1-4 with a mean k value of ~1.02, the SKR data indicate the presence of dual modulations in both hemispheres (circular polarization states). In the southern data the northern and southern modulations are roughly comparable, of which Fischer et al. (2015) follow the northern, but, surprisingly, in the northern data the southern modulation is stronger than the northern, of which Fischer et al. (2015) duly follow the southern, thus leading to periods that are switched in sense relative to those derived from the magnetic data. While the nature of the northern (RH) SKR modulations thus remains unexpected, these results at least demonstrate a basic correspondence in periodicity between the magnetic oscillations and the SKR modulations in line with physical principle, as opposed to the disparate picture presented by Fischer et al. (2015).

3.3. Magnetic phases and periods derived in post-equinox intervals

We now turn to the post-equinox intervals following E1 characterized by abrupt ~100–200 day changes in magnetic field PPO properties, for which single linear northern and southern phases have been fitted to the N- and S-format magnetic data by Provan et al. (2013, 2014), thus yielding single values for the northern and southern periods in each such interval as shown in Fig. 2f. We now address Fischer et al.'s (2015) criticism of this procedure and of the results so derived.

As indicated in Section 2, the magnetic phases and periods shown in Fig. 2 during intervals D2 and E1, and for whole of the pre-equinox data, were derived by Andrews et al. (2012) using running linear directional statistics fits to the magnetic phase data taken 25 data points at a time, typically spanning ~200 days. The length of these data segments was chosen to reduce the scatter associated both with measurement uncertainties in the Rev-by-Rev phase determinations, and the significant phase modulations that occur in equatorial data at the lengthening beat period during E1. The modeled phase results are seen in Fig. 2d and e to provide an excellent overall account of these data. This procedure is evidently inappropriate during the later post-equinox intervals when Rev-to-Rev changes occur in the period at ~100–200 day intervals, however, since this would result in smoothing of the phase data and hence period, in a manner which would neither describe nor respect the abrupt changes that are a principal feature of these data. In these circumstances, Provan et al. (2013, 2014) chose to present single linear fits to the data segments between the abrupt changes (intervals E2, E3, and so on), as indicated above, and as shown here in Figs. 2, 3, and 5. We emphasize, however, that these individual fits have entirely the same character and employ similar ~100-200 day data segments as the running linear fits employed by Andrews et al. (2012) for the previous intervals.

Nevertheless, Fischer et al. (2015) criticize this procedure and the results derived therefrom (their Section 6.2), in particular pointing out the varying periods in interval E2 derived from the higher cadence SKR data, and state that the linear fits "result in large errors, much larger than the mathematical errors calculated". However, these comments lack appreciation of the physical meaning of the single periods derived by Provan et al. (2013, 2014), which provide an accurate estimate of the constant period that describes the total integrated change in PPO phase over the intervals involved. It is thus no accident, for example, that the higher cadence SKR data in E2 vary approximately equally about the single northern and southern periods derived from magnetic data by Provan et al. (2013, 2014), despite the variations in period apparent in the SKR data (see Fig. 3e).

To demonstrate the physical meaning of the periods derived from the magnetic data, we consider the total change of (either northern or southern) PPO phase $\Delta\Phi$ in some interval T between times t and $t+T$, during which the period $\tau(t)$ in general varies with time. Rearranging Eq. (3) and integrating yields

$$\Delta\Phi = 360 \int_t^{t+T} \frac{dt}{\tau(t)}, \tag{15a}$$

where as usual the angle is expressed in degrees. From Eq. (3) we may also define a "mean" constant period $\langle\tau\rangle$ that would give the same total change in phase over the interval

$$\langle\tau\rangle = \frac{360T}{\Delta\Phi}, \tag{15b}$$

such that substituting Eq. (15a) into (15b) yields

$$\frac{1}{\langle\tau\rangle} = \frac{\Delta\Phi}{360T} = \frac{1}{T}\int_t^{t+T} \frac{dt}{\tau(t)}. \tag{15c}$$

This expression thus defines the "mean" period in terms of the variable period $\tau(t)$ through a simple integral relationship. In terms of the phase plots shown in Fig. 2d and e relative to guide phases corresponding to fixed periods τ_g, the total change in phase over the interval can be expressed as

$$\Delta\Phi = \frac{360T}{\tau_g} - \Delta\psi, \tag{16}$$

where $\Delta\psi$ is the change in relative phase ψ between the beginning and end of the interval (see Eq. (2)). If, therefore, the linear fit to the phases in Figs. 2d and e spans total phase $\Delta\psi$ across the interval, as will be the case to a first approximation, then the period associated with the linear fit is exactly the "mean" period defined in terms of the variable period by the integral in Eq. (15c). If, however, the linear fit deviates from the true value of $\Delta\psi$ by $\delta(\Delta\psi)$, then it is readily shown from Eq. (15c) that the resulting error in $\langle\tau\rangle$ is

$$\delta(\langle\tau\rangle) \approx \frac{\langle\tau\rangle^2}{T}\frac{\delta(\Delta\psi)}{360}, \tag{17}$$

where $\delta(\Delta\psi)$ is expressed in degrees. Examination of the linear fits in Figs. 2d and e suggests that the "error" in $\Delta\psi$ might typically be ~45°, with the higher cadence SKR data in these intervals certainly confirming that no "whole cycles" are lost via period variations between Rev-to-Rev determinations of the magnetic phases. Then taking $\langle\tau\rangle \approx 10.67$ *h* and $T \approx 200$ *days* yields an uncertainty in the mean period of $\delta(\langle\tau\rangle) \approx 0.003$ *h* (i.e., ~10 s), entirely compatible with the simple order of magnitude estimate given in point (a) at the end of Section 2. This value is also compatible with the uncertainties in period previously quoted by

Provan et al. (2013, 2014) for the linear fit analyses, the origins of which are outlined below.

In addition to measurement uncertainties, however, some of the phase deviations about the linear fits are due to short-term variations in the PPO periods, characterised by near-equal deviations in the phase of all three field components, previously termed "common jitter" by Provan et al. (2013). It is interesting then to note that related variations can also be directly detected in the SKR phase data, as in the southern data in interval E2. This finding suggests that determinations of the magnetic phases and periods at higher temporal resolution might be possible during some intervals, though still limited by the low Rev-to-Rev cadence of the data and the phase modulations due to beat effects. However, this does not mean that the single periods derived by Provan et al. (2013, 2014) are "problematical" as claimed by Fischer et al. (2015). Rather, as shown by the above analysis, the single periods have a specific physical meaning as given by the integral mean in Eq. (15), with uncertainties that are entirely in line with those previously quoted.

Given this discussion, however, it is appropriate here to briefly outline the analysis leading to the quoted uncertainties for individual linear fits, based on the standard error of a least-squares fit. We also compare this with the above analysis leading to Eq. (17). The linear fits are obtained by finding the pair of values (α, β) for which the linear model $\psi'(t) = \alpha t + \beta$ best fits a selected set of N phase values, ψ_k at time t_k (strictly speaking the phases involved are the N- and S-format phases $(\psi_i - \gamma_{i\,N,S})$ introduced in Section 2). The period relates specifically to the phase gradient α, for which we thus wish to estimate the uncertainty. The best linear fit is determined by minimising the variance V between the selected data and the model line, suitably defined as

$$V = \frac{1}{N}\sum_{k=1}^{N}(1 - \cos(\delta\psi_k)), \tag{18}$$

where $\delta\psi_k = (\psi_k - \psi'_k)$, and ψ'_k is the linear model value $\psi'_k = \alpha t_k + \beta$ at time t_k (see Section 5 of Andrews et al. (2012)). For phase deviations from the line that are not too large we may approximate the cosine in Eq. (18) by the leading terms in its expansion to yield

$$V \approx \frac{1}{2N}\sum_{k=1}^{N}\delta\psi_k{}^2 = \frac{1}{2}\overline{\delta\psi^2}, \tag{19}$$

where the angles are expressed in radians and the bar indicates the averaged value. Eq. (19) shows that the procedure is equivalent to a least-squares fit in the case of non-circular data, with a resulting root mean square (RMS) deviation about the best-fit line of $\delta\psi_{rms} \approx \sqrt{\overline{\delta\psi^2}_{min}} \approx \sqrt{2V_{min}}$ radians, an expression valid provided V_{min} does not significantly exceed ~0.5, corresponding to a limiting RMS deviation not significantly exceeding ~1 rad. The standard error in the slope of the fit is then given by (for N large compared with 2)

$$\delta\alpha \approx \sqrt{\frac{\overline{(\psi_k - \psi'_k)^2}}{N\overline{(t_k - \bar{t}_k)^2}}}, \tag{20}$$

and it is readily shown that for data spread approximately uniformly in time over total interval T we have $\overline{(t_k - \bar{t}_k)^2} \approx T^2/12$. The uncertainty in the slope of the fit is thus given by

$$\delta\alpha \approx \sqrt{\frac{12}{N}}\frac{\delta\psi_{rms}}{T} \approx \sqrt{\frac{24\,V_{min}}{NT^2}}. \tag{21}$$

Inserting this into Eq. (3) then yields the corresponding uncertainty in period as

$$\delta\tau \approx \frac{\tau^2}{2\pi}\delta\alpha \approx \frac{\tau^2}{\pi T}\sqrt{\frac{6V_{min}}{N}}, \tag{22}$$

which is the expression employed in previous studies by Provan et al. (2013, 2014). As indicated above, this expression is valid for minimum variances V_{min} that do not significantly exceed ~0.5. In general, minima are increasingly less well-defined for more scattered data with larger minimum variances than this.

For comparison with Eq. (17) above, we may also equivalently express the uncertainty in period in terms of the RMS angular deviation of the data about the best-fit line

$$\delta\tau \approx \sqrt{\frac{12}{N}}\frac{\tau^2}{T}\frac{\delta\psi_{rms}}{360}, \tag{23}$$

where $\delta\psi_{rms}$ is now expressed in degrees for comparison with Eq. (17). Bearing in mind that the number of phase data points N employed in each fit is typically ~24, comparison of Eq. (23) with Eq. (17) shows that the two estimates are closely related, with the effective uncertainty in the phase deviation across the interval associated with the linear fit being given by $\delta(\Delta\psi) \approx \sqrt{12/N}\delta\psi_{rms} \approx \delta\psi_{rms}/\sqrt{2}$. The simple connection indicated by this result, between the uncertainty in total phase deviation across an interval and the RMS deviation of the data about the fitted line, appears generally reasonable. By way of example we consider the fit to the N-format phase data for interval E3 in Fig. 2, for which we find $V_{min} \approx 0.2$, corresponding to $\delta\psi_{rms} \approx 35^\circ$. Then for $\tau \approx 10.63\ h$, $T \approx 225\ days$, and $N = 21$ we find from Eq. (22) an uncertainty in period of $\delta\tau \approx 0.002\ h$ as reported by Provan et al. (2013, 2014), entirely in line with the above discussion leading to Eq. (17).

3.4. Southern oscillations in interval E3

We finally turn to the discussion given by Fischer et al. (2015) of the magnetic phase data in interval E3, and their statement (their Appendix D) that the analysis of Provan et al. (2013, 2014) did not take into account "the intricate behavior of magnetic phases for constant phase differences". Examining Fig. 3a, it can be seen that in interval E3 the northern (RH) SKR modulation forms bands falling slowly with time, indicating a period slightly smaller than the 10.64 h period of the guide phase. Similarly, in Fig. 3b the southern (LH) modulation forms bands falling rapidly with time, indicating a period significantly smaller than the 10.70 h period of the guide phase, which Fischer et al. (2015) show correspond to a common phase-locked period with the northern modulation as seen in Fig. 3e. Fig. 3c also shows that the magnetic phase data in E3 are closely organized in N-format about the best-fit straight line, with some notable deviations in the middle of the interval, and are also in close "agreement" with the (-90° shifted) northern SKR maxima, this being the accidental consequence of the post-noon location of spacecraft apoapsis during this interval with effective dominant near-noon SKR sources, as discussed in Section 3.1. Accordingly, in Fig. 5a the northern magnetic and (RH) SKR phases in E3 are seen to be in very close correspondence, while in Fig. 5d the guide-phase transformed (and 180° shifted) northern magnetic phases similarly correspond very closely to the (+90° shifted) southern (LH) SKR modulations and phase, as then expected. We note that these findings are in complete agreement with the prior results of Provan et al. (2014), who found that SKR modulations with closely similar periods are present in both LH and RH polarized data in E3 (their Fig. 5c and d), with the same relation to the northern magnetic phase as described above (their Fig. 7d), but attributed this, as in Cowley and Provan (2015), to the dual SKR modulation effect first described by Lamy (2011).

Since the N-format magnetic phases of the three field components in E3 are closely similar, as can be seen in Fig. 3c, the near-equatorial oscillations in this interval have essentially pure "northern" polarization. That is, the φ component is (as always) in lagging quadrature with r, while the θ component is in antiphase with r (see Fig. 1b), brought to a common phase in Fig. 3c by the N-format phase adjustments defined in Section 2, by 90° for the φ component and 180° for the θ component. In Fig. 3d we then see that in S-format the θ component phases lie closely along the (+90° shifted) southern (LH) SKR maxima, while the (r, φ) phases lie ~180° apart, closely along southern (LH) SKR minima. Fischer et al. (2015) claim (their Section 6.2 and Appendix D) that these data provide evidence for the presence of a southern oscillation with the same period but in antiphase with the northern, compatible with the phase-locked common periods found in the SKR data, for which the S-format (r, φ) phases can be "corrected" by a 180° phase shift to bring them into line with the S-format θ phases (red arrows in their Fig. 12b).

This argument, however, is readily shown to be entirely fallacious. Suppose we have a pure "northern" oscillation of (for simplicity) fixed period in the magnetic data, in the complete absence of a southern oscillation, and that it has the same period as the northern (RH) SKR modulations, as expected. Then the magnetic phase data in N-format will lie along a common line, parallel to the northern SKR phase and emission maxima, displaced from it by some fixed phase $\Delta\psi$ (modulo 360°) in a plot such as Fig. 3c (nearly zero in E3), whose value is determined by the LT of spacecraft apoapsis as discussed in Section 3.1. Suppose further that the same SKR modulation is also present in the southern (LH) SKR data, as in E3, due, e.g., to the dual modulation effect noted by Lamy (2011). Then in S-format the (r, φ) phases, which are unchanged relative to N-format, will automatically form a common line also displaced by $\Delta\psi$ (modulo 360°) from the southern (LH) SKR phase and emission maxima, while the θ component phases, which are displaced 180° relative to N-format, will similarly automatically form a common line displaced by 180° from the (r, φ) phases, and hence displaced by $\Delta\psi \pm 180°$ (modulo 360°) from the southern (LH) SKR phase and emission maxima. This result concerning the relative phase displacements applies independently of the guide phases employed for the northern and southern data, of course, which simply changes the slope of the lines in the corresponding plots but not their relative phase. However, we must also recall that, following Fischer et al. (2015), the northern and southern SKR phases in Fig. 3c and d are shifted by 180° relative to each other (by -90° for the northern data in Fig. 3c and by +90° for the southern data in Fig. 3d) as discussed in Section 2 and Section 3.1, with the net effect that it is then the S-format θ component phases that will automatically lie along a common line displaced by $\Delta\psi$ (modulo 360°) from the southern (LH) SKR phase, while the (r, φ) component phases will similarly be automatically displaced by $\Delta\psi \pm 180°$ (modulo 360°). In Fig. 3c the N-format phases are seen to form a common line, consistent with an essentially pure northern oscillation, which "agrees" closely with the (-90° shifted) northern (RH) SKR phase and emission maxima, such that in this case we have $\Delta\psi \approx 0°$. Then the above discussion shows that in S-format the θ component phases will automatically lie along the dual modulated southern SKR maxima, while the (r, φ) component phases will similarly be automatically displaced through 180° to lie along the SKR minima, as in Fig. 3d. This phase configuration is exactly that produced by a pure northern oscillation alone, which thus provides no evidence whatever for the existence of a southern oscillation of the same period as claimed by Fischer et al. (2015). The 180° "correction" they discuss in relation to the red arrows in their Fig. 12b is just the inverse operation to the 180° shift in θ phases between S-format and N-format, which transforms the S-format data in Fig. 3d back into the common-line N-format data in Fig. 3c (though with a different guide phase), consistent with a pure northern oscillation, which again provides no evidence for the existence of a southern oscillation of the same period.

While the linear fit to the N-format data in Fig. 3c clearly provides an accurate measurement of the period of the northern magnetic oscillations, 10.633 ±0.002 h as determined by Provan et al. (2013) (see Section 3.3), no southern modulation could be detected in the S-format data by these authors. This indicates that if a southern oscillation is present with a distinctly different period to the northern, thus resulting in phase modulation through at least a half beat period during the interval, then its amplitude must be less than ~20% of that of the dominant northern oscillations (Provan et al., 2013). The difference in period required for this condition to be met is at least ~0.01 h, such as would certainly be the case for a southern oscillation with a period near to that in intervals E2 or E4 on either side (~10.69 h). Instead, the S-format data in E3, in which the (r, φ) phases and the θ phases are separated by ~180°, form "perfectly un-banded" phase data with a directional statistics variance close to unity to which no straight line fit can be made (see Andrews et al. (2012) their Section 5.4), since for each point in the data set (a combined (r, φ) phase point, say) another point exists at the same time t which differs in phase by ~180° (the corresponding θ phase point). For this reason Provan et al. (2013) reported no determination of the southern period during interval E3 of a similar nature to the periods reported for the other post-equinox intervals. Instead, they interpolated a possible southern phase across E3 from the end of E2 to beginning of E4, yielding a period very close to the southern period in the latter interval, with the expectation that other data sets, e.g., SKR, might be investigated in relation to this estimate. In the event, no modulation near this period, or at any other than the northern period, has been found in interval E3 in the southern (LH) SKR data either by Provan et al. (2014) or Fischer et al. (2015), such that the interpolated phase and period have not been repeated here.

As previously discussed by Cowley and Provan (2015), however, it is in principle possible that a southern oscillation (θ component in phase with r) with a period closely similar to the northern, which would not result in significant phase modulations over the interval, is indeed present in the magnetic data as Fischer et al. (2015) assert, even if the phase data provide no evidence for its presence one way or the other, contrary to their assertions. Two conditions must, however, be satisfied. The first is that the southern oscillation must either be close to in phase or to antiphase with the northern oscillation to retain the ~180° phase difference between the (r, φ) and θ component phases as observed, not just antiphase as indicated by Fischer et al. (2015) (though this would be directly compatible with in phase rather than antiphase SKR modulations as in Fig. 1c and d). The second is that the amplitude must be less than that of the northern oscillation, otherwise the combined oscillation would be transformed into a pure "southern" oscillation in terms of relative component phases, with the combined r component oscillating in phase with the combined θ component. Although such a southern oscillation may thus in principle be present as far as the phase data are concerned, Cowley and Provan (2015) have pointed out that this would also produce an effect in the relative magnitudes of the (r, φ) and θ component amplitudes. Specifically it would yield larger combined (r, φ) amplitudes and smaller combined θ amplitudes if the oscillations are in phase, and vice versa if the oscillations are in antiphase. However, Cowley and Provan (2015) have shown that the relative amplitudes of the (r, φ) and θ components in this interval do not differ significantly from values observed earlier in the mission when two distinct periods are present, from which they show that if such a common period southern oscillation is indeed present in E3, its

amplitude can be no more than ~5–10% of that of the northern oscillation.

We finally note that Fischer et al. (2015) also provide a similar discussion of the magnetic field phases during the second half of interval E1, when they again derive only a phase-locked common period from the SKR data as shown in Fig. 3e. They point out that the phase difference between the (r, φ) and θ components is less than ~180° in this case, actually closer to ~90°, and suggest that this is due to the addition of northern and southern magnetic oscillations of the same period, compatible with their result, that have a phase difference other than the ~180° they discuss for E3. However, they fail to notice the ~180° phase jumps that occur sequentially in the (r, φ) and θ component phase data during this interval (see Fig. 2d and e following Andrews et al. (2012) and Provan et al. (2013)), which result in the relative phases in these field components switching sequentially between +90° and -90°. This is the unequivocal signature produced by the beating of two oscillations of differing period but near-equal amplitude, with phase switches that occur every half beat period. Corresponding beat modulations are also present in the oscillation amplitude data, as shown in Fig. 2h–j, also following Andrews et al. (2012) and Provan et al. (2013). We thus conclude with Cowley and Provan (2015) that the phase-locked common northern and southern periods deduced by Fischer et al. (2015) in this interval again result from the dual modulation effect first reported by Lamy (2011), which in this case does not reflect the dual separated periods clearly revealed by the magnetic measurements.

4. Summary and conclusions

In this paper we have addressed a number of important issues concerning the PPO phenomenon in Saturn's magnetosphere, specifically the relationships between the post-equinox properties of the magnetic field oscillations discussed by Andrews et al. (2012) and Provan et al. (2013, 2014) and the SKR modulations reported by Fischer et al. (2014, 2015), for which significantly different results on basic properties such as the seasonally-varying northern and southern PPO periods have been reported. Resolution of such apparently discrepant results is important because the physical picture of the PPO phenomenon that has emerged from these and other studies (e.g., Fig. 1) suggests that the periods of the oscillations in the magnetic and SKR data should be essentially identical. Furthermore, investigation of the phase relationship between the magnetic oscillations, which are known to form perturbations that rotate around the planet at the PPO period (Cowley et al., 2006; Andrews et al., 2010a), and that of the SKR modulations, provides insight into the origins of the latter modulations, and whether these also form a rotating system like the magnetic, or whether they are mainly clock-like (strobe) as suggested by Fischer et al. (2015). Our principal results are summarized as follows.

(a) On the basis of physical principle we expect the periods of the magnetic oscillations and SKR modulations to be identical, apart from small differences (~10 s) resulting from the neglect of rotation effects in deriving SKR periods (see point (e) below), and have been shown to be so in the pre-equinox interval studied by Andrews et al. (2011, 2012). Very different results have nevertheless been reported for the immediate post-equinox interval from the magnetic field data by Andrews et al. (2012) and Provan et al. (2013, 2014), and from SKR data by Fischer et al. (2014, 2015). The northern and southern magnetic periods are robustly identified in the post-equinox near-equatorial data through the relative polarizations of the θ and (r, φ) field components, and furthermore show continuity with the converging single periods observed directly over the northern and southern polar regions during the immediately preceding pre-equinox interval of inclined orbits. From mid-August 2009 (near equinox) to mid-April 2010, however, the SKR periods deduced by Fischer et al. (2015) from tracking polarization-separated emission maxima "by hand" become approximately reversed in sense compared with the magnetic periods, south for north and vice versa. Examination of the SKR data during this interval, for which the northern and southern magnetic amplitudes are near-equal, reveals dual modulation at the two magnetic periods. For the southern (LH polarized) data the modulation at the two periods is roughly comparable, of which Fischer et al. (2015) follow the northern modulation, while previous analyses of these data by Lamy (2011) and Gurnett et al. (2011) follow the southern which thus agree well with the southern magnetic periods as found previously by Andrews et al. (2012). For the northern (RH polarized) data, however, the SKR modulation at the southern magnetic period is more distinct than that of the northern, and is hence followed by Fischer et al. (2015) to find "reversed" periods compared with the magnetic periods, except for some deviations mid-interval where the tracked northern SKR phase segues across adjacent southern magnetic cycles when this modulation becomes temporarily less distinct. While the dominance of the southern magnetic period in the northern (RH) SKR data remains unexpected, of course, the immediate post-equinox scenario outlined here does at least for the first time respect the principle of essentially identical magnetic and SKR periods in the immediate post-equinox interval, while at the same time also revealing issues concerning the analysis and interpretation of SKR data when dual modulation is present in polarization-separated data.

(b) In the post-equinox interval directly following the "reversed" periods, the southern magnetic period is found to dominate in both northern (RH) and southern (LH) SKR modulations in the interval between mid-April and early November 2010 when the southern magnetic oscillations were somewhat stronger than the northern, while the northern period is found to dominate both polarization channels between early November 2010 and mid-February 2011 when the northern magnetic oscillations were somewhat stronger than the southern. Consequently, Fischer et al. (2015) interpret the SKR data in these intervals as showing phase-locked common northern and southern periods, at first close to the southern magnetic period and later to the northern magnetic period, with a short interval of longer near-equal derived periods between as the "by hand" phase jumps between the two across a SKR data gap, while the magnetic data clearly show the presence of beat-modulated phases and amplitudes associated with two distinct slowly-varying periods. Our analysis thus supports the previous suggestion by Cowley and Provan (2015) that these results are due to dual modulation of the polarization-separated SKR emissions as previously discussed by Lamy (2011), with one modulation, northern or southern, dominating the other in both polarization channels, thus further illustrating the comments under point (a) above concerning the analysis and interpretation of SKR data post-equinox.

(c) The derived magnetic and SKR periods are in better overall agreement after mid-February 2011, when abrupt changes in oscillation amplitudes and periods occur in the magnetic data at ~100-200 day intervals (Provan et al, 2013). Due to the small but abrupt changes in period only single linear fits to each such segment of magnetic phase data were reported by Provan et al. (2013), which nevertheless have an

essentially similar character to the running ~200 day fits determined previously by Andrews et al. (2012). Fischer et al. (2015) have criticized these period determinations as showing large deviations relative to the sometimes variable periods determined from the higher cadence SKR data, such as in interval E2 from mid-February to mid-August 2011, with consequent "errors" that are significantly larger than the uncertainties quoted by Provan et al. (2013). However, their criticisms are misapplied due to lack of appreciation of the nature of the periods quoted, which, as we have proven here, provide an accurate estimate of the constant period that would yield the same total change in phase over each interval as a whole. The errors quoted by Provan et al. (2013) provide appropriate estimates of the uncertainties in these quantities.

(d) During interval E3, from mid-August 2011 to early April 2012, dual modulations are again observed in the northern (RH) and southern (LH) SKR data which Fischer et al. (2015) again interpret as phase-locked common northern and southern periods. During the same interval, however, only a northern oscillation with a period closely compatible with the SKR determinations was discerned by Provan et al. (2013), with the conclusion that any southern oscillation near the separate on-going southern period must be of much smaller amplitude, less than 20% of the northern. Fischer et al. (2015) argue that the S-format magnetic phase data provide evidence for the existence of a southern oscillation during this interval with the same period but in antiphase with the northern. We have shown that their argument is fallacious, the magnetic phase data provide evidence only for an oscillation with overall northern polarization (θ component in antiphase with r), and do not provide any evidence for the existence of a southern oscillation of the same period. In principle such an oscillation could be present, but as shown by Cowley and Provan (2015) from an analysis of the amplitude ratios between the spherical polar field components, if such an oscillation does exist its amplitude must be at least an order of magnitude smaller than the dominant northern oscillation, thus essentially negligible.

(e) We have further shown that the discussion given by Fischer et al. (2015) (their Section 6.2) concerning the relationship between the magnetic field and SKR phases is erroneous, the phase difference actually revealing the azimuth (LT) of the upward field-aligned currents of the northern and southern PPO current systems at corresponding SKR maxima. The claimed "agreement" with their erroneous argument during the later post-equinox interval is fortuitous, and implies only that the upward PPO currents are then located near noon at SKR maxima, with northern and southern equatorial field perturbations pointing to dusk and dawn, respectively. This relative phasing is an essentially accidental consequence of spacecraft apoapsis being located in the post-noon sector during this interval. As the latter statement implies, however, the phase relationship is found not to be fixed, but varies during the Cassini mission depending on the spacecraft orbit, principally with the LT of apoapsis for the usual elliptical orbits, and the consequent visibility of the conically-beamed SKR sources. Pre-equinox the northern and southern perturbation fields are instead directed toward noon and midnight, respectively, at corresponding SKR maxima (Provan et al., 2011; Andrews et al., 2011, 2012), implying the upward currents are then located near dawn, while immediately post-equinox (interval E1) they are reversed to point toward midnight and noon, implying upward currents at dusk at SKR maxima. These changing configurations relate to Cassini apoapsis being generally located in the dawn hemisphere pre-equinox and near dusk immediately post-equinox, then moving into the post-noon sector in the later post-equinox interval discussed by Fischer et al. (2015) as mentioned above. These results show conclusively that the SKR modulations are not mainly clock-like (strobe) as argued by Fischer et al. (2015), implying a fixed relationship between the magnetic and SKR phases, but instead rotate around the planet in a similar manner to the current systems as found by Lamy (2011), if in effect non-uniformly due to the strong variation of the source intensity with LT as discussed by Andrews et al. (2011).

Overall, the most important consequence of the detailed examination of the joint magnetic and SKR data set carried out in this paper is that it demonstrates the essential compatibility of the magnetic field and SKR PPO data in the post-equinox interval, despite the contrary results reported to date. The results also show that due to the dual modulation effect first described in polarization-separated SKR data by Lamy (2011), analysis and interpretation of such data may contain more subtleties than may initially have been appreciated. Joint examination of the combined magnetic and SKR data clearly provides greater insight and enhanced confidence compared with analyses of these data sets individually.

Acknowledgment

This work was supported by STFC Consolidated Grant ST/K001000/1. We thank Dr L Lamy for useful comments on post-equinox SKR properties. We also thank Mr G Hunt for provision of Fig. 1.

References

Andrews, D.J., Bunce, E.J., Cowley, S.W.H., et al., 2008. Planetary period oscillations in Saturn's magnetosphere: Phase relation of equatorial magnetic field oscillations and SKR modulation. J. Geophys. Res. 113, A09205 http://dx.doi.org/10.1029/2007JA012937.

Andrews, D.J., Cowley, S.W.H., Dougherty, M.K., et al., 2010a. Magnetic field oscillations near the planetary period in Saturn's equatorial magnetosphere: Variation of amplitude and phase with radial distance and local time. J. Geophys. Res. 115, A04212 http://dx.doi.org/10.1029/2007JA014729.

Andrews, D.J., Coates, A.J., Cowley, S.W.H., et al., 2010b. Magnetospheric period oscillations at Saturn: Comparison of equatorial and high-latitude magnetic field periods with north and south SKR periods. J. Geophys. Res. 115, A12252 http://dx.doi.org/10.1029/2010JA015666.

Andrews, D.J., Cecconi, B., Cowley, S.W.H., et al., 2011. Planetary period oscillations in Saturn's magnetosphere: Evidence in magnetic field phase data for rotational modulation of Saturn kilometric radiation emissions. J. Geophys. Res. 116, A09206 http://dx.doi.org/10.1029/2011JA016636.

Andrews, D.J., Cowley, S.W.H., Dougherty, M.K., et al., 2012. Planetary period oscillations in Saturn's magnetosphere: Evolution of magnetic oscillation properties from southern summer to post-equinox. J. Geophys. Res. 117, A04224 http://dx.doi.org/10.1029/2011JA017444.

Burch, J.L., DeJong, A.D., Goldstein, J., et al., 2009. Periodicity in Saturn's magnetosphere: Plasma cam. Geophys. Res. Lett. 36, L14203 http://dx.doi.org/10.1029/2009GL039043.

Burton, M.E., Dougherty, M.K., Russell, C.T., 2010. Saturn's internal planetary magnetic field. Geophys. Res. Lett. 37, L24105 http://dx.doi.org/10.1029/2010GL045148.

Carbary, J.F., Mitchell, D.G., Krimigis, S.M., et al., 2007. Electron periodicities in Saturn's outer magnetosphere. J. Geophys. Res. 112, A03206 http://dx.doi.org/10.1029/2006JA012077.

Cecconi, B., Lamy, L., Zarka, P., et al., 2009. Gonipolarimetric study of the revolution 29 perikrone using the Cassini Radio and Plasma Wave Science instrument high-frequency radio receiver. J. Geophys. Res. 114, A03215 http://dx.doi.org/10.1029/2008JA013830.

Cowley, S.W.H., Wright, D.M., Bunce, E.J., et al., 2006. Cassini observations of planetary-period magnetic field oscillations in Saturn's magnetosphere: Doppler shifts and phase motion. Geophys. Res. Lett. 33, L07104 http://dx.doi.org/10.1029/2005GL025522.

Cowley, S.W.H., Provan, G., 2015. Planetary period oscillations in Saturn's magnetosphere: Comments on the relation between post-equinox periods determined from magnetic field and SKR emission data. Ann. Geophys. 33, 901–912.

Desch, M.D., Kaiser, M.L., 1981. Voyager measurement of the rotation period of Saturn's magnetic field. Geophys. Res. Lett. 8, 253–256.

Fischer, G., Ye, S.-Y., Groene, J.B., et al., 2014. A possible influence of the Great White Spot on Saturn kilometric radiation periodicity. Ann. Geophys. 32, 1463–1476.
Fischer, G., Gurnett, D.A., Kurth, W.S., et al., 2015. Saturn kilometric radiation periodicity after equinox. Icarus 254, 72–91.
Galopeau, P.H.M., Lecacheux, A., 2000. Variations of Saturn's radio rotation period measured at kilometre wavelengths. J. Geophys. Res. 105, 13089–13101.
Gurnett, D.A., Kurth, W.S., Scarf, F.L., 1981. Plasma waves near Saturn: Initial results from Voyager 1. Science 212, 235–239.
Gurnett, D.A., Kurth, W.S., Hospodarsky, G.P., et al., 2005. Radio and plasma wave observations at Saturn from Cassini's approach and first orbit. Science 307, 1255–1259.
Gurnett, D.A., Lecacheux, A., Kurth, W.S., et al., 2009. Discovery of a north-south asymmetry in Saturn's radio rotation period. Geophys. Res. Lett. 36, L16102 http://dx.doi.org/10.1029/2009GL039621.
Gurnett, D.A., Groene, J.B., Persoon, A.M., et al., 2010. The reversal of the rotational modulation rates of the north and south components of Saturn kilometric radiation near equinox. Geophys. Res. Lett. 37, L24101 http://dx.doi.org/10.1029/2010GL045796.
Gurnett, D.A., Groene, J.B., Averkamp, T.F., et al., 2011. The SLS4 longitude system based on a tracking filter analysis of the rotational modulation of Saturn kilometric radiation. In: Rucker, H.O., Kurth, W.S., Louarn, P., Fischer, G. (Eds.), Planetary Radio Emissions VII. Austrian Acad. Sci. Press, Vienna, pp. 51–64.
Hunt, G.J., Cowley, S.W.H., Provan, G., et al., 2014. Field-aligned currents in Saturn's southern nightside magnetosphere: Sub-corotation and planetary period oscillation components. J. Geophys. Res. 119, 9847–9899 http://dx.doi.org/10.1002/2014JA020506.
Hunt, G.J., Cowley, S.W.H., Provan, G., et al., 2015. Field-aligned currents in Saturn's northern nightside magnetosphere: Evidence for interhemispheric current flow associated with planetary period oscillation components. J. Geophys. Res. 120, 7552–7584 http://dx.doi.org/10.1002/2015JA021454.
Jia, X., Kivelson, M.G., 2012. Driving Saturn's magnetospheric periodicities from the upper atmosphere/ionosphere: Magnetotail response to dual sources. J. Geophys. Res. 117, A11219 http://dx.doi.org/10.1029/2012JA018183.
Kaiser, M.L., Desch, M.D., Kurth, W.S., et al., 1984. Saturn as a radio source. In: Gehrels, T., Matthews, M.S. (Eds.), Saturn, Space Science Series. Univ. Arizona Press, Tucson, Arizona, pp. 378–415.
Kimura, T., Lamy, L., Tao, C., et al., 2013. Long-term modulations of Saturn's auroral radio emissions by the solar wind and seasonal variations controlled by the solar ultraviolet flux. J. Geophys. Res. 118, 7019–7035. doi:10.1002/2013JA018833.
Kurth, W.S., Averkamp, T.F., Gurnett, D.A., et al., 2008. An update to a Saturnian longitude system based on kilometric radio emissions. J. Geophys. Res. 113, A05222. doi:10.1029/2007JA012861.
Lamy, L., 2011. Variability of southern and northern SKR periodicities. In: Rucker, H.O., Kurth, W.S., Louarn, P., Fischer, G. (Eds.), Planetary Radio Emissions VII. Austrian Acad. Sci. Press, Vienna, pp. 39–50.
Lamy, L., Zarka, P., Cecconi, B., et al., 2008a. Saturn kilometric radiation: Average and statistical properties. J. Geophys. Res. 113, A07201 http://dx.doi.org/10.1029/2007JA012900.
Lamy, L., Zarka, P., Cecconi, B., et al., 2008b. Modeling of Saturn kilometric radiation arcs and equatorial shadow zone. J. Geophys. Res. 113, A10213 http://dx.doi.org/10.1029/2008JA013464.
Lamy, L., Cecconi, B., Prangé, R., et al., 2009. An auroral oval at the footprint of Saturn's kilometric radio sources, co-located with the UV aurorae. J. Geophys. Res. 114, A10212 http://dx.doi.org/10.1029/2009JA014401.
Lamy, L., Schippers, P., Zarka, P., et al., 2010. Properties of Saturn kilometric radiation measured within its source region. Geophys. Res. Lett. 37, L12104 http://dx.doi.org/10.1029/2010GL043415.
Lamy, L., Cecconi, B., Zarka, P., et al., 2011. Emission and propagation of Saturn kilometric radiation: Magnetoionic modes, beaming pattern, and polarization state. J. Geophys. Res. 116, A04212 http://dx.doi.org/10.1029/2010JA016195.
Provan, G., Andrews, D.J., Arridge, C.S., et al., 2009. Polarization and phase of planetary period oscillations on high latitude field lines in Saturn's magnetosphere. J. Geophys. Res. 114, A02225 http://dx.doi.org/10.1029/2008JA013782.
Provan, G., Andrews, D.J., Cecconi, B., et al., 2011. Magnetospheric period magnetic field oscillations at Saturn: Equatorial phase 'jitter' produced by superposition of southern- and northern-period oscillations. J. Geophys Res. 116, A04225 http://dx.doi.org/10.1029/2010JA016213.
Provan, G., Andrews, D.J., Arridge, C.S., et al., 2012. Dual periodicities in planetary period magnetic field oscillations in Saturn's tail. J. Geophys. Res. 117, A01209 http://dx.doi.org/10.1029/2011JA017104.
Provan, G., Cowley, S.W.H., Sandhu, J., et al., 2013. Planetary period magnetic field oscillations in Saturn's magnetosphere: Post-equinox abrupt non-monotonic transitions to northern system dominance. J. Geophys. Res. 118, 3243–3264 http://dx.doi.org/10.1002/jgra.50186.
Provan, G., Lamy, L., Cowley, S.W.H., et al., 2014. Planetary period oscillations in Saturn's magnetosphere: Comparison of magnetic oscillations and SKR modulations in the post-equinox interval. J. Geophys. Res. 119, 7380–7401. doi:10.1002/2014JA020011.
Smith, C.G.A., 2010. A Saturnian cam current system driven by asymmetric thermospheric heating. Mon. Not. R. Astron. Soc. 410, 2315–2329. doi:10.1111/j.1365-2966.2010.17602.x.
Southwood, D.J., Kivelson, M.G., 2007. Saturn magnetospheric dynamics: Elucidation of a camshaft model. J. Geophys. Res. 112, A12222 http://dx.doi.org/10.1029/2007JA012254.
Southwood, D.J., Kivelson, M.G., 2009. The source of Saturn's periodic radio emission. J. Geophys. Res. 114, A09201. doi:10.1029/2008JA013800.
Southwood, D.J., Cowley, S.W.H., 2014. The origin of Saturn magnetic periodicities: Northern and southern current systems. J. Geophys. Res. 119, 1563–1571. doi:10.1002/2013JA019632.
Warwick, J.W., Pearce, J.B., Evans, D.S., et al., 1981. Planetary radio astronomy observations from Voyager-1 near Saturn. Science 212, 239–243.
Ye, S.-Y., Gurnett, D.A., Groene, J.B., et al., 2010. Dual periodicities in the rotational modulation of Saturn narrowband emissions. J. Geophys. Res. 115, A12258 http://dx.doi.org/10.1029/2010JA015780.